Calculations of the conversion factor from organic carbon to organic matter for aerosol mass balance

Anna Font, Joel F. de Brito, Véronique Riffault, Sébastien Conil, Jean-Luc Jaffrezo, Aude Bourin

Atmospheric Pollution Research 15 (2024) 102301

Contents lists available at ScienceDirect

Atmospheric Pollution Research

journal homepage: www.elsevier.com/locate/apr

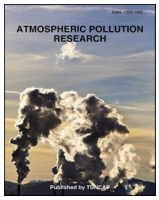

Calculations of the conversion factor from organic carbon to organic matter for aerosol mass balance

Anna Font [a,*], Joel F. de Brito [a], Véronique Riffault [a], Sébastien Conil [b], Jean-Luc Jaffrezo [c], Aude Bourin [a]

[a] IMT Nord Europe, Europe, Institut Mines-Télécom, Univ. Lille, Centre for Education, Research and Innovation in Energy Environnement (CERI EE), 5900, Lille, France
[b] ANDRA DISTEC/EES Observatoire Pérenne de l'Environnement, F-55290, Bure, France
[c] Institut des Géosciences de l'Environnement (IGE) CNRS, UGA, IRD, Grenoble INP, 38058, Grenoble CEDEX, France

ARTICLE INFO

Keywords:
Carbonaceous aerosol
Organic carbon
Organic matter
Conversion faction
$PM_{2.5}$ mass balance

ABSTRACT

Aerosol mass balance studies based on filter samples require a conversion factor to derive organic matter (OM) concentrations from organic carbon (OC) measurements from thermo-optical methods. This factor provides indirect insights on the molecular structure of OM needed in chemical transport models. Site- and season-specific ratios of OC to OM ($f_{OM:OC}$) were calculated using data from five rural background sites in France between 2012 and 2021 by relating the unidentified chemical fraction in $PM_{2.5}$ samples to thermo-optical OC concentrations. Further, multiple linear formulations were used to evaluate the impact of possible artefacts on the determination of $f_{OM:OC}$. The resulting $f_{OM:OC}$ was then compared to other estimates derived from online aerosol mass spectrometry data, showing good agreement. The spatial and temporal variability in $f_{OM:OC}$ is discussed considering factors such as seasonality, meteorological conditions and the atmospheric oxidative potential. Linear-mixed effect models were formulated to quantitatively determine the drivers which influence the $f_{OM:OC}$ at the French rural background sites. Both ozone and relative humidity were variables with statistically significant effects on $f_{OM:OC}$, indicating that differences in the contributions from both photooxidation and water content, explain the variability in $f_{OM:OC}$ observed at the French rural background sites. Site-specific $f_{OM:OC}$ yielded more accurate $PM_{2.5}$ mass closure and are therefore recommended in mass-balance exercises. Accurate $f_{OM:OC}$ are critical to maintain consistency in OM time series, especially in cases where filter-based time series may be replaced by state-of-the-art online instrumentation.

1. Introduction

Organic carbon (OC) and elemental carbon (EC) are the main carbonaceous aerosols found in ambient air, both constituting the predominant component in particulate matter (PM) across various environments including urban, rural and background sites (Christiansen et al., 2020; Querol et al., 2013; Weber et al., 2019; Yttri et al., 2009, 2021). OC, representing the major fraction of carbonaceous aerosols, can be emitted primarily from anthropogenic combustion sources including fossil and biomass fuels, and commercial cooking; as well as from natural sources such as plant debris, spores and pollens, among others. Secondary OC (SOC) is formed through the oxidation of volatile organic compounds (VOCs) from both natural and anthropogenic sources. Under atmospheric conditions, VOCs may oxidize with ozone (O_3), nitrate (NO_3) and/or hydroxyl radicals (OH) to form less-volatile products which may undergo further reactions and/or partition into the condensed phase (Seinfeld and Pankow, 2003; Srivastava et al., 2022). These processes are affected by various factors such as temperature, relative humidity and total organic aerosol mass loadings (e.g., Hennigan et al., 2009). OC, together with EC, secondary inorganic aerosols (SIA) and major ions, are monitored at rural background sites as required by the European Air Quality Directive (European Parliament & Council of the European Union, 2008) for the characterization of the main components of $PM_{2.5}$ (PM with a mean aerodynamic diameter <2.5 μm). Carbonaceous aerosols are associated with adverse health effects, including cardiovascular and respiratory diseases (Janssen et al., 2012; Mauderly and Chow, 2008), neurodegenerative and carcinogenic effects, among others (Aslam and Roeffaers, 2022); they also have an

Peer review under responsibility of Turkish National Committee for Air Pollution Research and Control.
* Corresponding author.
E-mail address: anna.font@imt-nord-europe.fr (A. Font).

https://doi.org/10.1016/j.apr.2024.102301
Received 17 May 2024; Received in revised form 2 September 2024; Accepted 2 September 2024
Available online 3 September 2024

impact on the climate system with OC and EC having a cooling and warming effect, respectively (IPCC, 2021).

Traditionally, the quantification of OC (and EC) in PM involves thermo-optical methods applied to air samples collected on quartz fibre filters. Different temperature protocols specify the temperature ramps to separate the OC and EC fractions. In Europe, the EUSAAR_2 protocol (Cavalli et al., 2010) was optimised for analysing carbonaceous aerosols at European regional background sites. However, OC quantified by thermo-optical methods does not account for other elements such as hydrogen, oxygen, nitrogen and sulphur present in organic aerosol. Often, organic matter (OM) is calculated by applying a constant OM/OC ratio (or $f_{OM:OC}$) to account for non-carbon organic mass. A conversion factor is also used in global and regional models to simulate primary organic aerosols from OC (Park et al., 2003). The chemical composition of OM varies with location, season, and time of day as the mix of organic compounds in the aerosol varies according to combustion efficiencies and the presence of primary and secondary OC (Brown et al., 2013; Turpin and Lim, 2001), making its estimation complex (Lim and Turpin, 2002). Conversion factors range from 1 (representing pure graphitic carbon) to 3.8 for aliphatic dicarbonyls (Simon et al., 2011; Turpin and Lim, 2001). OM/OC ratios larger than 3.8 might be possible, due to the presence of organic sulphates but the probability of such high ratio in ambient air is low due to low concentrations of such compounds (Simon et al., 2011). In between, carboxylic acids such as oxalate have ratios of 1.74; and that of levoglucosan is 2.25. $f_{OM:OC}$ also varies seasonally and larger ratios were found in summer when photochemical activity enhances the production of aged secondary organic aerosol (Bae et al., 2006; Hand et al., 2019; Malm et al., 2011; Ruthenburg et al., 2014; Simon et al., 2011). The most frequent approach in $PM_{2.5}$ mass balance studies is to use a single $f_{OM:OC}$ ratio which value is selected depending on the type of monitoring site. Low $f_{OM:OC}$ (1.2–1.4) is used for local and fresh sources (Timonen et al., 2013) but this ratio might differ in environments with large biomass burning emissions; whereas $f_{OM:OC}$ of 1.9–2.2 is typically used for sites with highly oxidized secondary organic aerosol (SOA) (Daellenbach et al., 2017). Lim and Turpin (2002) recommended a site-dependent $f_{OM:OC}$: 1.6 ± 0.2 and 2.1 ± 0.2 for urban and non-urban aerosols, respectively. In France, a general conversion factor of 1.8 is used (Golly et al., 2019). Despite the increasing availability of instruments measuring online OM in Europe (Bressi et al., 2021; Chen et al., 2022) and in France (Chebaicheb et al., 2023; Favez et al., 2021), OM continues to be routinely assessed by the OC proxy.

This manuscript evaluates the temporal and spatial variability in the factor used to convert OC to OM concentration, commonly used in PM mass balance studies at European regional background sites. The $f_{OM:OC}$ were calculated using the residual method applied to filter data collected at five rural background sites in France over the years 2012–2021. These ratios were then compared with the typically used fixed ratios, those from multi-linear regression models and those derived from online aerosol mass spectrometry. The variability of $f_{OM:OC}$ was analysed in relation to the instrumentation used to measure $PM_{2.5}$ mass concentrations, weather conditions, and the oxidative capacity of the atmosphere.

2. Methods

2.1. Monitoring sites, instruments, $PM_{2.5}$ chemical composition and other data

Data used here comprises $PM_{2.5}$ mass concentrations and basic chemical composition monitored at five rural background sites in France in 2012–2021 (Fig. 1). The site Andra-OPE (OPE; 48°34′N, 05°30′E; 392 m altitude; EMEP/FR0022) is an atmospheric station part of a long-term environmental monitoring system in the framework of a deep geological disposal facility for radioactive residues (http://www.andra.fr/ope/) in the north-east of France. The largest town in the region, Nancy, is located 50 km NE of the site with over 100,000 inhabitants. The Atlantic Ocean is 350 km away from the site. Peyrusse-Vieille (PEY; 43°47′N, 00°11′E; 236 m; EMEP/FR0013) is in the south-west of France, 250 m away from the centre of a village with less than 100 inhabitants. It is 130 km away from the Atlantic Ocean, 45 km from the forest of Landes (dominated by maritime pine trees) and 32 km from the closest town (22,000 inhabitants). Revin (REV; 49°54′N, 04°38′E; 390 m; EMEP/FR0009) is in the middle of a coniferous forest with the nearest village (890 inhabitants) 1.5 km SSW of the monitoring site. The town of Revin (6000 inhabitants) is located 4.5 km north of the site. The North Sea is 190 km away. St Nazaire-Le Désert (SND; 44°34′N, 5°17′E; 605 m; EMEP/FR0023) is a few kilometres SE of the centre of a 200 inhabitants'

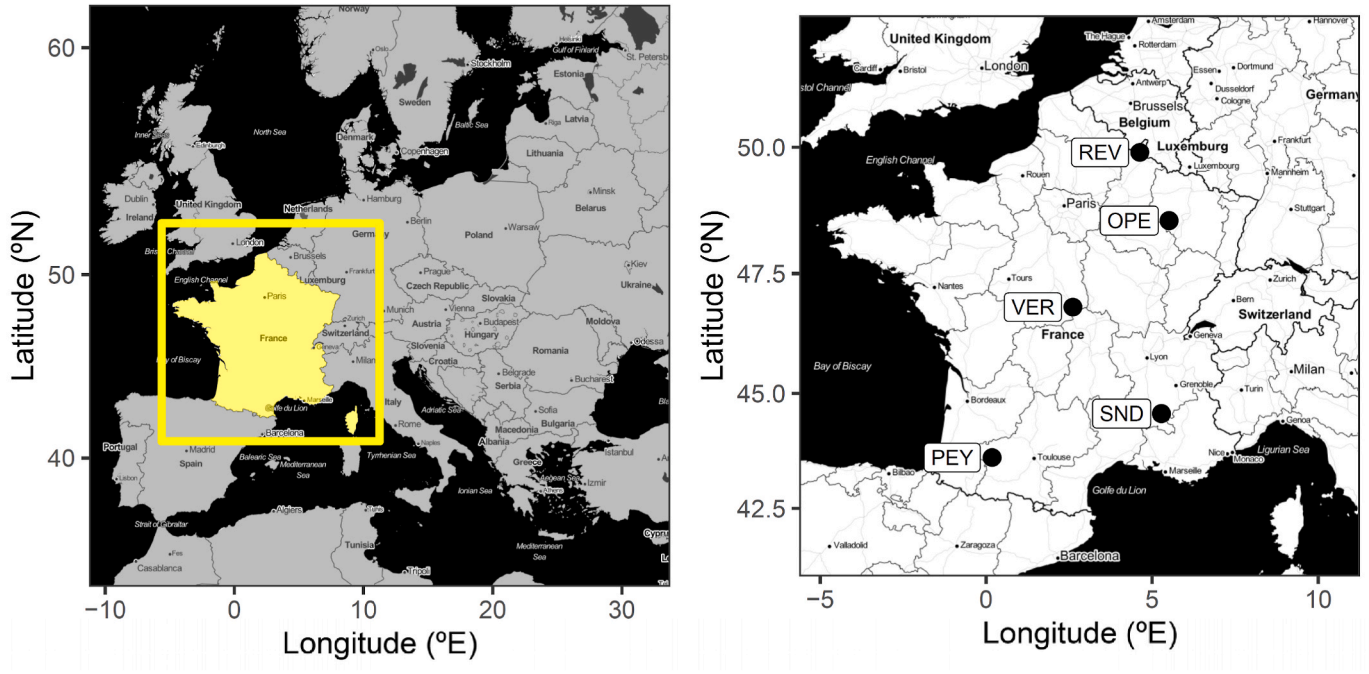

Fig. 1. Europe with mainland France highlighted in yellow (left) and a map with the location of the French rural background sites monitoring $PM_{2.5}$ chemical composition in 2012–2021 (right).

village in the SE of France, with a landscape dominated by forest and agricultural fields. The Mediterranean Sea is 150 km south of the monitoring site with Marseille (~900,000 inhabitants) on the coast and the city of Lyon (500,000 inhabitants) 215 km NNW. Verneuil (VER; 46°49′N, 2°37′E; 182 m; EMEP/FR0025) is in the centre of France, 230 km south of Paris and 300 km from the Atlantic Ocean and 400 km from the Mediterranean Sea. The surroundings are characterized by more than 50% of forest and grassland and also influenced by the nearby timber industry. PEY, REV, SND and VER belong to the French National Observatory of Measurement and Evaluation in Rural Areas (MERA) managed locally by the relevant regional Approved French Air Quality Monitoring Associations (AASQA) and nationally by IMT Nord Europe. The OPE station is managed by ANDRA with support from Atmo Grand Est.

Hourly $PM_{2.5}$ gravimetric mass was monitored by either a Tapered Element Oscillating Microbalance-Filter Dynamics Measurement System (TEOM-FDMS; Thermo R&P; USA); a Beta Attenuation Monitor 1020 (BAM, MetOne Instruments Inc; USA); a beta gauge MP101MRST (ENVEA; France) or a FIDAS 200 (PALAS; Finland), depending on the site and year. All instruments have mechanisms to remove the water content from the incoming air. Change of instrumentation took place at all sites in the time series (Fig. S1) and the time series was maintained given that all instruments are accredited to measure PM-equivalent mass concentrations in France on a 24-h average basis (LCSQA, 2013, 2017). Daily $PM_{2.5}$ mass concentrations were calculated from hourly measurements with at least 75% data capture. Ozone (O_3) was also measured hourly. Data collection and validation of the automatic analysers were conducted by the regional AASQA as part of the French Air Quality Monitoring Program.

Quartz fibre filters (Pallflex Tissuquartz 2500 QAT-UP, 150 mm in diameter) were pre-fired for 24 h before sampling to remove organic impurities at 1073 K at OPE; and at 773 K at the MERA sites. The latter was done according to the PD CEN/TR 16243:2011 guidelines. Similar filter pre-fired conditions were applied in other European studies (Sciare et al., 2003; Viana et al., 2006; Pio et al., 2020). Sample filters were exposed to ambient air for 24 h using a High-Volume Sampler (Digitel DAH-80) equipped with a $PM_{2.5}$ inlet and sampling at a rate of 30 m^3 h^{-1}. Samplers were placed inside a temperature-controlled monitoring cabin (20–23 °C) to limit the loss of semi-volatile species. After sampling, filters were stored at temperatures < 4 °C and shipped back to the laboratories for chemical analysis. Great care is taken to avoid contamination and filter modification at all steps of sampling and handling. A total of 2176 filters were analysed over the study period for organic and elemental carbon (OC, EC) and major inorganic ions (Ca^{2+}, K^+, Mg^{2+}, Na^+, NH_4^+; and Cl^-, NO_3^-, SO_4^{2-}). OC-EC was quantified by Thermo-Optical Reflectance by the Sunset analyser (Sunset Laboratory, Inc, USA) following the EUSAAR2 temperature protocol (Cavalli et al., 2010). Water-soluble inorganic ions were quantified by digesting a punch of the filter in pure water and then analysed by ion chromatography (Ca^{2+}, K^+, Mg^{2+}, Na^+, NH_4^+; and Cl^-, NO_3^-, SO_4^{2-}). At the MERA sites, field blanks were collected monthly, averaged seasonally and removed from ambient samples for the inorganic ions but not for OC and EC. Laboratory blanks for each filter lot were analysed monthly to quantify the limit of detection (LoD) and limit of quantification (LoQ). LoD was calculated as the standard deviation times the inverse of the student's law (95%). LoQ was three times LoD. At OPE, field blanks were collected every 2–3 weeks, averaged annually and removed from samples for all species, including OC and EC. LoQ was calculated from the annual field blank plus twice its standard deviation. For all sites, whenever the sample was below the LoQ, it was substituted by LoQ/2.

Collocated in-situ non-refractory PM_1 chemical composition (including OM, sulphate, nitrate, and ammonium) was conducted at times at REV. An aerosol mass spectrometer (AMS, Aerodyne Research Inc., USA; 5-min resolution) sampled in summer 2012 (24 Jun-14 Jul), and a quadruple Aerosol Chemical Speciation Monitor (Q-ACSM, Aerodyne Research Inc., USA; 30-min resolution) (Ng et al., 2011) in winter 2017-18 (28 Nov–3 Apr). Daily filters were collected for the winter campaign and analysed using the same procedures as for the fortnight filter samples described before.

Temperature (T) and relative humidity (RH) were measured at OPE, PEY and REV. For SND and VER, T and RH were extracted from the nearest meteorological site from the NOAA the Integrated Surface database network (Smith et al., 2011) accessed through the worldmet R-package (Carslaw, 2019).

2.2. $f_{OM:OC}$ calculations

$PM_{2.5}$ mass balance calculations are based on the assumption that total $PM_{2.5}$ mass concentrations can be expressed as the sum of its main components:

$$PM_{2.5} = [OM] + [EC] + [SIA] + [sea\ salt] + [dust] + [trace\ elements] + \varepsilon \quad (1)$$

where OM stands for organic matter, and SIA for secondary inorganic aerosols which include nitrate, non-sea salt-sulphate and ammonium. Trace elements include metals and other trace elements. ε refers to the residual term including the missing mass, errors associated with the on-line $PM_{2.5}$ instruments and the analytical errors of the chemical analysis.

Sea salt concentrations (ss) were calculated from the following tracers:

$$[sea\ salt] = [ss\text{-}Na^+] + [Cl^-] + [ss\text{-}Mg^{2+}] + [ss\text{-}Ca^{2+}] + [ss\text{-}K^+] + [ss\text{-}SO_4^{2-}] \quad (2)$$

Ratios used in Eq. (2) were $[ss\text{-}Ca^{2+}] = 0.038 \times [ss\text{-}Na^+]$; $[ss\text{-}K^+] = 0.037 \times [ss\text{-}Na^+]$; and $[ss\text{-}SO_4^{2+}] = 0.252 \times [ss\text{-}Na^+]$ as in Seinfeld and Pandis (2006).

To separate $ss\text{-}Na^+$ from the non-sea salt Na^+ ($nss\text{-}Na^+$), the Na-to-Ca ratio in crust $(Na/Ca)_{crust} = 0.56$ Bowen (1979) as reported in Marconi et al., 2014) was used, and the following set of equations was formulated:

$$[nss\text{-}Na^+] = [nss\text{-}Ca^{2+}] \times (Na/Ca)_{crust} \quad (3)$$

$$[ss\text{-}Na^+] = [Na^+] - [nss\text{-}Na^+] \quad (4)$$

$$[nss\text{-}Ca^{2+}] = [Ca^{2+}] - [ss\text{-}Ca^{2+}] \quad (5)$$

Resolving the system of equations and using the representative ratios:

$$[nss\text{-}Ca^{2+}] = 1.022 \times [Ca^{2+}] - 0.039 \times [Na^+] \quad (6)$$

$$[nss\text{-}Na^+] = 0.57 \times [Ca^{2+}] - 0.0212 \times [Na^+] \quad (7)$$

Dust concentrations were calculated from non-sea-salt calcium ($nss\text{-}Ca^{2+}$) as $[dust] = 9.7 \times [nss\text{-}Ca^{2+}]$. $nss\text{-}Ca^{2+}$ was calculated as per Eq. (6). The conversion factor that relates dust and $nss\text{-}Ca^{2+}$ used here was calculated using the data from an intensive measurement campaign in winter 2013, where a wide spectrum of elements related to crustal content (Al, Si, Fe, Ti and P) was monitored at three French sites. PM_{10} daily filters were collected and analysed and dust concentrations assessed (see Alastuey et al. (2016) for details about the methodology). The relation between $nss\text{-}Ca^{2+}$ and mineral dust calculated from crustal elements was consistent at the three sites and the inverse of the slope (9.7) used as a conversion factor (Fig. S2).

Non-sea salt sulphate in SIA was calculated by subtracting the sea salt component, as shown before, from total sulphate. Only the non-sea-salt-non-dust potassium ($nss\text{-}ndust\text{-}K^+$) was included as other trace metals and elements were not routinely analysed at the MERA sites. $nss\text{-}ndust\text{-}K^+$ was calculated subtracting the sea-salt and dust component from total potassium. The readers are referred to Font et al. (2024) for further details.

OM was estimated from OC as:

$$[OM] = f_{OM:OC} \times [OC] \quad (8)$$

where $f_{OM:OC}$ is the conversion factor from OC to OM. The mass closure approach or residual method (RM) was used to estimate it, assuming that $PM_{2.5}$ mass closure can be explained by major sources (marine, dust, SIA, EC and trace elements) and the unaccounted $PM_{2.5}$ fraction (or residual $PM_{2.5}$ mass) is then attributed to OM. The normalisation of this component to OC provides an estimation of the conversion factor or $f_{OM:OC}$ (Bae et al., 2006; Cesari et al., 2014; El-Zanan et al., 2005; Guinot et al., 2007):

$$f_{OM:OC} = ([PM_{2.5}] - ([EC] + [SIA] + [sea\ salt] + [dust] + [nss\text{-}ndust\text{-}K^+]) / OC \quad (9)$$

The conversion factor here represents the upper-limit value due to the non-accounted mass in the chemical composition data (i.e., metals associated with industrial emissions, etc). The entire dataset ($N = 2176$ filters) was used to estimate $f_{OM:OC}$. First, $f_{OM:OC}$ was calculated daily from individual samples as well by linear models. Different types of regressions were tested: ordinary least square (OLS), OLS regression with a forced zero intercept, and the Reduced-Major-Axis (RMA) regression. OLS regression minimizes residuals in the *y*-axis (i.e., unaccounted $PM_{2.5}$ mass $= [PM_{2.5}] - ([EC] + [SIA] + [sea\ salt] + [dust] + [nss\text{-}ndust\text{-}K^+])$ whereas the RMA regression minimizes both *x* (i.e., OC) and *y* (i.e., unaccounted $PM_{2.5}$ mass) residuals. The latter is preferred in atmospheric applications when relating two measured variables (e.g., Ayers, 2001) as both *x* and *y* have associated errors.

Alternatively, $f_{OM:OC}$ was estimated using a multi-linear regression (MLR) relating $PM_{2.5}$ mass residual against multiple $PM_{2.5}$ elements, including OC. Multiple MLRs were formulated (Table 1). As per Hand et al. (2019); Malm et al. (2011); and Malm and Hand (2007), ammonium sulphate (AS) and ammonium nitrate (AN) were calculated from sulphate and nitrate concentrations, respectively, considering that both sulphate and nitrate were fully neutralized and solely in the form of ammonium sulphate and ammonium nitrate, respectively. Calculations used here were $[AS] = 1.375 \times [nss\text{-}SO_4^{2-}]$ and $[AN] = 1.29 \times [NO_3^-]$ (Hand et al., 2019). EC was not included as an explanatory variable in any of the multi-linear models due to collinearities with OC (Hand et al., 2019). Similarly, NH_4^+ was not included in the MLR due to its correlation with both nitrate and sulphate. Note that models #6 and #7 are essentially the same but AN and AS in model #7 were calculated from individual ions including NH_4^+. Model #7 is essentially the RM as per Eq. (9). Coefficients from the MLR were also used to evaluate possible sampling and analytical artefacts (Hand et al., 2019; Malm and Hand, 2007). The coefficients derived from the regressions are interpreted as mass multipliers that account for unmeasured compounds and/or effects of potential sampling or analytical biases (Hand et al., 2019). The coefficient for OC (a_1 as in Table 1) is equivalent to $f_{OM:OC}$.

Table 1
Different multi-linear models were considered to estimate $f_{OM:OC}$. $PM_{2.5}$ residual concentrations were calculated taking into account different PM species depending on the model.

	Residual considered	ML-model
#1	$PM_{2.5}$ – EC	residual ~ $0 + a_1 \times OC + a_2 \times AN + a_3 \times AS + a_4 \times nss\text{-}ndust\text{-}K^+ + a_5 \times dust + a_6 \times sea\_salt$
#2	$PM_{2.5}$ – (EC + sea_salt)	residual ~ $0 + a_1 \times OC + a_2 \times AN + a_3 \times AS + a_4 \times nss\text{-}ndust\text{-}K^+ + a_5 \times dust$
#3	$PM_{2.5}$ – (EC + sea_salt + *nss-ndust*-K^+)	residual ~ $0 + a_1 \times OC + a_2 \times AN + a_3 \times AS + a_5 \times dust$
#4	$PM_{2.5}$ – (EC + sea_salt + *nss-ndust*-K^+ + dust)	residual ~ $0 + a_1 \times OC + a_2 \times AN + a_3 \times AS$
#5	$PM_{2.5}$ – (EC + sea_salt + *nss-ndust*-K^+ + dust + AS)	residual ~ $0 + a_1 \times OC + a_2 \times AN$
#6	$PM_{2.5}$ – (EC + sea_salt + *nss-ndust*-K^+ + dust + AS + AN)	residual ~ $0 + a_1 \times OC$
#7	$PM_{2.5}$ – (EC + sea_salt + *nss-ndust*-K^+ + NH_4^+ + dust + nss-SO_4^{2-} + NO_3^-)	residual ~ $0 + a_1 \times OC$

Further, $f_{OM:OC}$ calculated from filter data was compared to those derived from the in-situ instrumentation at REV. For summer 2012, an AMS instrument provided OM:OC ratios derived from the HR peak fitting procedure implemented in the PIKA module of the AMS software program (Aiken et al., 2007). For winter 2017, daily $f_{OM:OC}$ were calculated from the OM mass concentrations measured by a Q-ACSM and relating them against the OC obtained by thermo-optical measurements on filters. OM from the Q-ACSM was reported every half an hour and averaged daily. A 75% data threshold was applied to calculate daily means.

2.3. Linear-mixed effect regression modelling to understand the drivers of $f_{OM:OC}$

Linear-mixed effect regression modelling was used to understand the drivers that explain the variability in $f_{OM:OC}$ observed across the French rural background sites. The $f_{OM:OC}$ calculated by the residual method (i.e., Eq. (9)) at each monitoring site was taken as the outcome, averaged by long periods covering the different times that $PM_{2.5}$ mass concentrations were monitored by the different type of instruments at each monitoring site (Fig. S1). A random effect was specified on each monitoring site. The *lmer* function from the lme4/R package (version 1.1.34) (Bates et al., 2015) was used. The 95% confidence intervals for the fixed effects were calculated using the *confint* function using the Wald method (i.e., central estimate ± 1.96 x standard error) from the stats/R package (version 4.3.1). A fixed effect (or explanatory variable) was considered significant (i.e. driving $f_{OM:OC}$) whenever its confidence interval did not include zero.

Several model formulations were tested and compared against the null model (without fixed effects). Before building the model, possible collinearity between fixed effects was assessed by means of the pairwise Pearson correlation values and the maximum variance inflation factor (VIF). Thresholds of $R > 0.70$ and VIF >10 are suggested thresholds indicating possible collinearity (see references in Dormann et al. (2013)). Only explanatory variables with $R < 0.70$ were included in the model formulation and the model was kept whenever the maximum VIF value was < 10.

The best model was selected based on the Conditional Akaike Information (cAIC); the model fit or correlation coefficient (R^2); and the Likelihood Ratio Test (LRT). The best model was selected compromising the three criteria: the lowest cAIC, the highest R^2 with an LRT test significant at least at $p < 0.05$.

3. Results and discussion

3.1. $f_{OM:OC}$ from filter data

Chemical data from all filters were used to calculate $f_{OM:OC}$ as per Eq. (9). Median $f_{OM:OC}$ ranged from 1.4 (SND) to 3.2 (PEY) with intermediate values of 1.8 (REV) and 2.3 (OPE and VER) (Table 2). For the OLS regression forced to zero, the correlations between the residual $PM_{2.5}$ *vs* OC were moderate to strong at all sites (range R^2: 0.56–0.84), indicative of a significant dependency of the $PM_{2.5}$ residual to OC concentrations. SND was the site with the lowest slope (i.e., $f_{OM:OC}$) (1.5) followed by OPE (1.8), REV (2.1), VER (2.3) and PEY (2.9) (Table 2). The coefficient of determination was however weaker for the other type of regressions (range of $R^2 = 0.16$–0.57), indicating a lower fraction of OC was explained by the $PM_{2.5}$ residuals. The OLS regression returned the lowest slopes or $f_{OM:OC}$ (range of 1.0–2.1) while RMA regression had the largest (range of 2.5–3.7). The OLS regression forced to origin showed better correlation coefficients and slopes closer to the median $f_{OM:OC}$ from daily observations (Table 2). Also, the resulting conversion factors were in agreement with those expected in ambient data (1.4–2.3) according to (Turpin and Lim, 2001). The adjusted R^2 for the multi-linear models are shown in Fig. S8 and ranged from $R^2 = 0.52$ to $R^2 = 0.95$. Generally, model #6 and model #7 showed the lowest R^2 compared to the rest of

Table 2
$f_{OM:OC}$ calculated from median daily (residual $PM_{2.5}$ mass)/OC ratios; by ordinary-least-square (OLS) regression of residual $PM_{2.5}$ mass vs OC; OLS regression with a forced zero intercept; reduced-major-axis regression (RMA) and multi-linear regression (median from models #1 to model#5) and coefficients from model #6 (Table 1). CI stands for confidence interval.

	RM				MLR	
Site	Median ratio [p25-p75][a]	OLS regression: [95% CI]; R^2	OLS - forced to origin: [95% CI]; R^2	RMA regression: [95% CI]; R^2	Multi-linear regression: median [min, max] Min R^2 – Max R^2	Multi-linear regression (model #6): [95% CI]; R^2
OPE	2.3 [1.4; 3.2]	1.0 [0.8; 1.3]; $R^2 = 0.16$***	1.8 [1.6; 2.0]; $R^2 = 0.56$***	2.6 [2.3; 2.8]; $R^2 = 0.16$***	1.8 [1.6; 2.2] $R^2 = 0.83$–0.90***	1.7 [1.5; 1.9]; $R^2 = 0.52$***
PEY	3.2 [2.7; 3.6]	2.1 [1.8; 2.3]; $R^2 = 0.36$***	2.9 [2.8; 3.0]; $R^2 = 0.77$***	3.4 [3.2; 3.7]; $R^2 = 0.36$***	2.0 [1.9; 2.6] $R^2 = 0.84$–0.91***	2.9 [2.7; 3.0]; $R^2 = 0.77$***
REV	1.8 [1.5; 2.0]	1.7 [1.4; 2.0]; $R^2 = 0.21$***	2.1 [2.0; 2.2]; $R^2 = 0.62$***	3.7 [3.4; 4.0]; $R^2 = 0.21$***	1.5 [1.4; 1.9] $R^2 = 0.85$–0.92***	2.1 [2.0; 2.3]; $R^2 = 0.62$***
SND	1.4 [1.2; 1.5]	1.3 [1.1; 1.5]; $R^2 = 0.28$***	1.5 [1.4; 1.6]; $R^2 = 0.70$***	2.5 [2.3; 2.7]; $R^2 = 0.28$***	1.3 [1.2; 1.5] $R^2 = 0.79$–0.91***	1.5 [1.4; 1.5]; $R^2 = 0.70$***
VER	2.3 [2.1; 2.4]	2.1 [1.9; 2.2]; $R^2 = 0.57$***	2.3 [2.2; 2.4]; $R^2 = 0.84$***	2.7 [2.6; 2.9]; $R^2 = 0.57$***	1.9 [1.9; 2.2] $R^2 = 0.92$–0.95***	2.3 [2.2; 2.4]; $R^2 = 0.81$***

*** regression statistically significant at $p < 0.001$.
[a] *p25* and *p75* refers to the first and third quartile, respectively.

models at the same site. $f_{OM:OC}$ estimated from the MLR model #1 to model #5 (Table 1) were similar (Fig. S8) and summarized together in Table 2. $f_{OM:OC}$ ranged from 1.6 to 2.2 at OPE (median: 1.8); 1.9–2.9 at PEY (median: 2.0); 1.4–1.9 at REV (median: 1.5); 1.2–1.5 at SND (median: 1.3); 1.9–2.2 at VER (median: 1.9) (Table 2). $f_{OM:OC}$ estimated from the MLR were slightly lower than the ratios calculated by the RM by either the OLS forced to zero or the RMA regression (Table 2) and they were particularly low at REV (1.5) and SND (1.3). This indicates that part of the sampling and analytical artefacts might be transferred to the $f_{OM:OC}$ ratio estimated by the RM. Coefficients for OC from the MLR from model #6 did not differ from that from model #7 and equalled that from the RM (Table 2; Fig. S8). This indicates that both nitrate and sulphate were fully neutralized by ammonium and validate the calculation of AS and AN.

OLS regression forced to zero yielded larger correlations between the $PM_{2.5}$ residuals and OC than the other types of regressions when considering the 2012–2021 data for the estimation of $f_{OM:OC}$ using the RM method. $f_{OM:OC}$ calculated from the MLR varied depending on the elements considered as explanatory variables. Therefore, the RM method with the OLS regression forced to zero was considered as a more robust method to calculate representative site-specific $f_{OM:OC}$.

The site-specific $f_{OM:OC}$ for SND and OPE was below the recommended value of 2.1 for non-urban environments (Lim and Turpin, 2002). However, lower $f_{OM:OC}$ were previously calculated at these types of monitoring sites (Chow et al., 2015). Low $f_{OM:OC}$ (1.5–1.6) were also previously calculated at a French regional background site near Paris (20 km) in July 2009 (Crippa et al., 2013) and in 2011–2013 (Petit et al., 2015) (Table 3). Also, at the remote mountain site of Jungfraujoch (3580 m in the Swiss Alps), $f_{OM:OC}$ was 1.84 in winter 2005 (Cozic et al., 2008). In Cabauw, The Netherlands, $f_{OM:OC}$ was 1.6 in PM_1 (Liu et al., 2024). REV and VER exhibited a range of values representative of highly oxidized OM, which agreed with the expected ratio of 2.1 for non-urban aerosols. Similar ratios (2.0–2.1) were calculated for three rural sites in the Ile-de-France region for 2009–2010 (Bressi et al., 2013), and for VER ($f_{OM:OC} = 2.07$) in 2011-14 (He et al., 2018) (Table 3). PEY had the largest $f_{OM:OC}$ ratio, slightly above the 2.2–2.6 range representative for non-urban sites according to Lim and Turpin (2002) but in agreement with the presence of highly oxidized aerosols. Comparing the site-specific $f_{OM:OC}$ between sites, only OPE and VER observed statistically similar ratios, probably related to their continental location (Fig. 4A), with the ocean located more than 300 km away (Fig. 1).

Seasonal $f_{OM:OC}$ were slightly different compared to the long-term conversion factors and the variation was not homogeneous among sites (Fig. S3). The largest $f_{OM:OC}$ was in spring at OPE, PEY and VER (2.2–3.2), whereas at REV it was in winter (2.4), and in summer at SND (1.7). The lowest $f_{OM:OC}$ were calculated in summer at OPE, PEY and REV (1.4, 2.7 and 1.8, respectively) and in autumn at SND (1.3). VER showed comparable values (2.2–2.3) in all seasons except spring (2.6). Considering the daily variability in $f_{OM:OC}$ by seasons, OPE and SND showed non-statistical differences among seasons (Fig. S4B). Similarly, (Bressi et al., 2013) observed a lack of clear seasonal variation in the $f_{OM:OC}$ ratio at five sites in the Ile-de-France region, including one urban (Paris), one suburban and three rural sites (Table 3). For the other sites (PEY, REV and VER), summer $f_{OM:OC}$ was generally statistically different from the other seasons and generally lower (Fig. S4B). This seasonal behaviour of $f_{OM:OC}$ contrasts with those previously reported in the literature for the same type of monitoring sites. Previous studies in the US and in Europe highlighted the seasonal variation of $f_{OM:OC}$, with more elevated $f_{OM:OC}$ in summer and lower in winter, consistent with more aged secondary organic aerosol in the warm periods associated with enhanced photochemical activity; and less aged primary organic aerosol in winter (El-Zanan et al., 2005; Hand et al., 2019; Malm et al., 2011; Malm and Hand, 2007; Poulain et al., 2020; Ruthenburg et al., 2014; Simon et al., 2011). However, large $f_{OM:OC}$ values were also observed in the cold season in Pittsburgh, US (Polidori et al., 2008) and was related to biomass burning and residential wood combustion. The biomass burning contribution to OC concentrations was estimated to be 40–90% at French rural background sites in winter 2013 (Golly et al., 2019). Primary organic markers of biomass burning, such as levoglucosan, are characterized by large $f_{OM:OC}$ (2.25) (Chow et al., 2018), and there is evidence of secondary organic aerosols formed from residential wood burning in ambient measurements (Mohr et al., 2012). Oxygenated organic aerosols from biomass burning emissions were reported at suburban sites in the north of France (Chebaicheb et al., 2023; Roig Rodelas et al., 2019), and elsewhere (Wallace et al., 2018), consistent with elevated $f_{OM:OC}$, with ratios of 1.93 (Roig Rodelas et al., 2019) and 2.03 (Wallace et al., 2018).

3.2. Investigation of samples outside expected $f_{OM:OC}$

Following the residual method, about 38% of all filters used here were out of the expected 1–4 range for $f_{OM:OC}$: 3% had a negative $f_{OM:OC}$ (i.e. the sum of chemical composition was too high); or $f_{OM:OC}$ was < 1 (17%) or > 4 (18%) (Table S1). Per sites, $f_{OM:OC} > 4$ represented the majority of cases (14–34% of the total observations) except at SND where the largest proportion was for $f_{OM:OC} < 1$ (26%) (Table S1). $f_{OM:OC} > 4$ was more frequent in January–May, and $f_{OM:OC} < 1$ in summer (Fig. S6A) but without large differences. Samples with $f_{OM:OC} < 0$ (i.e., negative residuals and therefore $PM_{2.5}$ larger than the reconstructed mass) were characterised by significantly larger concentrations of nitrate and dust compared to samples with $f_{OM:OC}$ within the expected range ($1 < f_{OM:OC} < 4$) (Fig. S7), suggesting a possible overestimation of

Table 3
Values of $f_{OM:OC}$ reported in the literature in various studies at remote sites.

Reference	Particle size	Location (type), Country	Method	Period	$f_{OM:OC}$
Kiss et al. (2002)	$PM_{1.5}$	K-puszta (rural background), Hungary	Total organic carbon (TOC) analyser to determine TC and WSOC. Used solid-phase extraction on a copolymer sorbent. Analysed C, H, N, and S of OM by elemental analyser with estimated O	Jan–Sep 2000	1.93 ± 0.038 (range: 1.9–2.0)
El-Zanan et al. (2005)	$PM_{2.5}$	Multiple sites (rural background), US	Residual method applied to 24 h filters. OC quantified using the TOR thermal protocol	1998–2003	2.07 (all); 2.33 (summer); 1.87 (winter)
Cozic et al. (2008)	PM_1, TSP	Jungfraujoch (remote), Switzerland	OM PM_1 by Q-AMS *vs* filter-based OC TSP by the Sunset instrument, following the NIOSH protocol	Feb–Mar 2005	1.84
Lowenthal et al. (2009)	$PM_{2.5}$	Great Smoky Mountains (remote), US	OM measured gravimetrically to OC measured by thermal optical reflectance in residues of isolated WSOC	Jul–Aug 2006	2.4 ± 0.3
Takahama et al. (2011)	PM_1	Whistler mountain (remote), Canada	FTIR and ACSM	Mar–Apr 2019	2.0–2.2
Bressi et al. (2013)	$PM_{2.5}$	3 sites around Paris (rural), France	Residual method applied on 24 h filters. OC by the Sunset instrument, following the EUSAAR 2 protocol	Sep 2009–Sep 2010	Urban site: 1.95; Suburban site: 1.98; North-east rural: 2.08; North-west rural: 2.03; South rural: 2.12; Seasonal: 1.8–2.2
Crippa et al. (2013)	PM_1	SIRTA (regional background), France	AMS	Jul 2019	1.66 ± 0.11 (Whole period); 1.68 ± 0.11 (Atlantic clean); 1.62 ± 0.09 (Atlantic polluted); 1.72 ± 0.04 (Continental)
Petit et al. (2015)	PM_1, $PM_{2.5}$	SIRTA (regional background), France	OM PM_1 by Q-ACSM vs filter-based OC $PM_{2.5}$ by the Sunset instrument, following the EUSAAR2 protocol	Jun 2011–Jun 2013	1.49 ± 0.04
Ruthenburg et al. (2014)	$PM_{2.5}$	Multiple sites (rural background), US	FTIR	2011	1.71–1.83 (all); 1.64 (winter); 1.70 (spring); 1.71 (summer, autumn)
He et al. (2018)	$PM_{2.5}$	Verneuil (rural background), France	Residual method applied on 24 h filters. OC by the Sunset instrument, following the EUSAAR 2 protocol	2011–2014	2.066
Hand et al. (2019)	$PM_{2.5}$	Multiple locations (rural background), US	Multi-linear regression relating $PM_{2.5}$ residual concentrations to OC. OC quantified using the TOR optical thermal protocol	2005–2016	1.67 (2005–2010); 1.46 (2005–2010: winter); 1.69 (2005–2010: spring); 1.83 (2005–2010: summer); 1.68 (2005–2010: autumn); 1.86 (2011–2016); 1.60 (2011–2016: winter); 1.86 (2011–2016: spring); 2.05 (2011–2016: summer); 1.88 (2011–2016: autumn)
Poulain et al. (2020)	PM_1	Melpitz (rural background), Germany	OM PM_1 by Q-ACSM *vs* filter-based OC PM_1 by the Sunset instrument, following the EUSAAR2 protocol	Jun 2012–Nov 2017	1.71 (all); 1.29 (winter); 1.84 (spring); 2.74 (summer); 2.49 (autumn)
This study	$PM_{2.5}$	Verneuil (rural background), France	Residual method (OLS regression) applied on 24 h filters. OC by the Sunset instrument, following the EUSAAR 2 protocol	2014–2021	2.3 (all); 2.2 (winter); 2.6 (spring); 2.3 (summer, autumn)
This study	$PM_{2.5}$	Revin (rural background), France	Residual method (OLS regression) applied on 24 h filters. OC by the Sunset instrument, following the EUSAAR 2 protocol	2014–2021	2.1 (all); 2.1 (winter); 2.4 (spring); 2.8 (summer); 1.9 (autumn)
This study	$PM_{2.5}$	Revin (rural background), France	AMS	Summer 2012	1.8
This study	$PM_{2.5}$	Revin (rural background), France	OM PM_1 by Q-ACSM *vs* filter-based OC $PM_{2.5}$ by the Sunset instrument, following the EUSAAR2 protocol	Winter 2017	2.2
Liu et al. (2024)	PM_1	Cabauw (rural background), The Netherlands	Average daily OM PM_1 by TOF-ACSM-CV-$PM_{2.5}$ divided by the filter-based OC PM_1 by the Sunset instrument, following the EUSAAR2 protocol	11–May 24, 2021 and 16 Sep – Oct 12, 2021	1.58 ± 0.54
Liu et al. (2024)	$PM_{2.5}$	Cabauw (rural background), The Netherlands	Average daily OM $PM_{2.5}$ by TOF-ACSM-CV-$PM_{2.5}$ divided by the filter-based OC $PM_{2.5}$ by the Sunset instrument, following the EUSAAR2 protocol	11–May 24, 2021 and 16 Sep – Oct 12, 2021	1.97 ± 0.59

TSP: total suspended particles; WSOC: water soluble organic carbon.

both. This agrees with Galindo et al. (2020) which observed that the chemical mass closure on PM_{10} samples at a location in south-east Spain on days with Saharan dust outbreaks were lower than concentrations measured gravimetrically. This was associated with a lower conversion factor to estimate dust concentration from *nss*-Ca^{2+}. Samples with $f_{OM:OC} < 0$ were also characterised by lower OC concentrations. Samples with $f_{OM:OC} > 4$ were characterised by lower concentrations of both OC and EC as well as *nss-ndust*-K^+ compared to samples with $1 < f_{OM:OC} < 4$ (Fig. S7). The Wilcox test indicates that both *nss*-SO_4^{2-} and NH_4^+ were statistically different in samples with $f_{OM:OC} > 4$, but the median concentrations were 16% and 24% lower, respectively (Fig. S7). There was, however, a clear inter-annual distribution of unexpected $f_{OM:OC}$ (Fig. S6B) that coincided with the $PM_{2.5}$ instrument used with larger $f_{OM:OC}$ associated with TEOM-FDMS (Fig. S1), resulting with different $f_{OM:OC}$ depending on the type of instrument used to measure $PM_{2.5}$ mass concentrations (Fig. S5). All $PM_{2.5}$ instruments complied with the EU reference method and no correction to $PM_{2.5}$ mass is suggested (LCSQA, 2013). Removing those filters with a daily $f_{OM:OC}$ not in the 1–4 range resulted in slightly lower $f_{OM:OC}$ at PEY (2.5); and larger values at OPE and SND (2.0 and 1.8, respectively) for the 2012–2021 period. At REV and VER, ratios were similar (2.1 and 2.2, respectively).

3.3. Sampling and analytical artefacts

The coefficients for AN and AS from the MLR were used to evaluate possible sampling and analysis artefacts as presented in Hand et al. (2019); Malm et al. (2011)). Coefficients were expected to be 1 for perfect mass closure. However, multiple artefacts may exist. $PM_{2.5}$ mass concentrations can be overestimated due to inefficient drying systems leading to the presence of particle bound water (PBW) associated with inorganic salts and other water-soluble species such as AN and AS, leading to coefficients > 1 (Bae et al., 2006; Malm et al., 2011). Other possible positive artefacts comprise the absorption of acid gases to the filter tape used in some $PM_{2.5}$ analysers. This was previously reported for the BAM-1020 systems (Le et al., 2020; Liu et al., 2013). Conversely, $PM_{2.5}$ mass concentrations may be biased low due to the volatilisation of semi-volatile organics or ammonium nitrate. It is well documented in the literature that AN might volatilise from the filter media including quartz fibre filters (Chow et al., 2015; Keck and Wittmaack, 2005; Bae et al., 2006a; Malm et al., 2011), glass fibre filters such as those used in the Met One BAM-1020 (Le et al., 2020; Liu et al., 2013), and Teflon-coated glass fibre filters used by the TEOM-FDMS systems (Salvador and Chou, 2014). However, some studies have pointed an overestimation of the $PM_{2.5}$ mass by TEOM-FDMS due to the chilled filter holding too much volatile PM (Schwab et al., 2006). Other negative artefacts may be related to the PALAS-FIDAS instrument missing particle mass associated with particles smaller than 0.18 μm, its lower particle cut-off.

Globally, the coefficient for AS was above 1 at all French rural background sites for all the MLR models tested (Fig. S8D) indicating the possible influence of PBW or acid gases associated with the presence of sulphate or sulphur compounds. By type of instrument, the coefficient for AS ranged from 1.0 for the BETA instrument; to 1.9 for the FIDAS (Table 4). The coefficients for AN were 1.4–1.7 at PEY using the 2012–2021 data indicating a possible influence of volatilisation of NH_4NO_3 particles at this site from either the quartz fibre filters (Fig. S8C) or an overestimation of the semi-volatile PM leading to larger $PM_{2.5}$ concentrations from the online instrument. The artefact associated with AN at PEY was present independently of the type of instrument used (PALAS-FIDAS and TEOM-FDMS), although the artefact was larger for the PALAS-FIDAS (1.6 [1.4–1.9]) than the TEOM-FDMS (1.3 [1.0–1.6]) (Fig. 3). The coefficients were 0.8–0.9 at OPE; and 0.7–0.8 at SND indicating possible losses of semi-volatile material by the $PM_{2.5}$ online instrument by 10–30%, respectively (Fig. S4C). Conversely, at REV and VER, the coefficient was approximately 1.

From Fig. S5 and Table 4 it is clear that the type of instrument to measure $PM_{2.5}$ mass concentrations had an effect on the determination of $f_{OM:OC}$. To better understand the artefacts associated with the $PM_{2.5}$ instruments, MLR was calculated for each type of instrument and site. Coefficients associated with OC, AN and AS from model #4 are shown in Fig. 2. All instruments showed coefficients for AS > 1, the lowest being for the BAM1020 (median: 1.3) and the largest for the FIDAS (median: 1.9) (Fig. 2C). Coefficients for AN were 0.7 for the MP101M, 1.0 for the BETA, 1.1 for both the TEOM-FDMS and the BAM1020 and 1.6 for the FIDAS (Fig. 2B). FIDAS was the instrument with the largest coefficients for both AS (median: 1.9) and AN (median: 1.6) (Fig. 2).

Malm et al. (2011) stated that the coefficient for AN from the MLR included the artefacts associated with PBW and volatilisation and argued that if the coefficient for AS is considered as representative of the first artefact also for AN, the fraction of volatilised nitrate could be estimated. Here, we calculated the artefact associated with the PBW associated with AN by comparing the coefficient for AN from the MLR when AS was considered as an explanatory variable (model #4) with that without (model #5) (Table 4). In general, the coefficient for AN from model #5 was slightly larger than that from model #4, but only by 6% (range: 0–10%) (Table 4), with differences independent of the monitoring site and instrument type (Fig. S9). This indicates that any possible artefact related to PBW was not associated with AN and mainly with AS. However, the coefficient for OC (or $f_{OM:OC}$) increased by 16% (range: 8–39%) when AS was removed from the MLR, with the FIDAS and the MP101M showing the greatest impact (increase by 39% and 33%, respectively) (Table 4). The introduction of AS in the $PM_{2.5}$

Table 4
Coefficients with 95% confidence interval in brackets estimated from the MLR models #4, #5 and #6 for OC, ammonium nitrate (AN) and ammonium sulphate (AS) and differences in coefficients associated with the different types of instruments.

Instrument	Element	Coefficient model #4	Coefficient model #5	Coefficient model #6	Difference coefficient Model #4 vs #5 (%)	Difference coefficient Model #5 vs #6 (%)
TEOM-FDMS	OC	2.1 [1.9–2.3]	2.4 [2.3–2.6]	2.3 [2.2–2.4]	17	−4
	AN	0.9 [0.8–0.9]	0.9 [0.8–1.0]		8	
	AS	1.5 [1.4–1.7]	–			
MP101M	OC	1.0 [0.9–1.2]	1.4 [1.3–1.5]	1.3 [1.2–1.4]	33	−8
	AN	0.7 [0.7–0.6]	0.7 [0.6–0.9]		10	
	AS	1.6 [1.4–1.8]	–			
BETA	OC	1.6 [1.2–2.0]	1.9 [1.7–2.2]	1.9 [1.7–2.1]	17	0
	AN	1.0 [0.8–1.1]	1.0 [0.9–1.2]		5	
	AS	1.4 [0.9–1.9]	–			
BAM1020	OC	1.8 [1.7–2.0]	1.9 [1.7–2.0]	2.0 [1.9–2.0]	3	6
	AN	1.1 [1.0–1.2]	1.1 [1.0–1.2]		0	
	AS	1.1 [0.9–1.3]	–			
FIDAS	OC	1.4 [1.1–1.6]	1.9 [1.8–2.1]	2.2 [2.1–2.4]	39	14
	AN	1.9 [1.7–2.1]	2.0 [1.7–2.2]		5	
	AS	2.0 [1.7–2.4]	–			

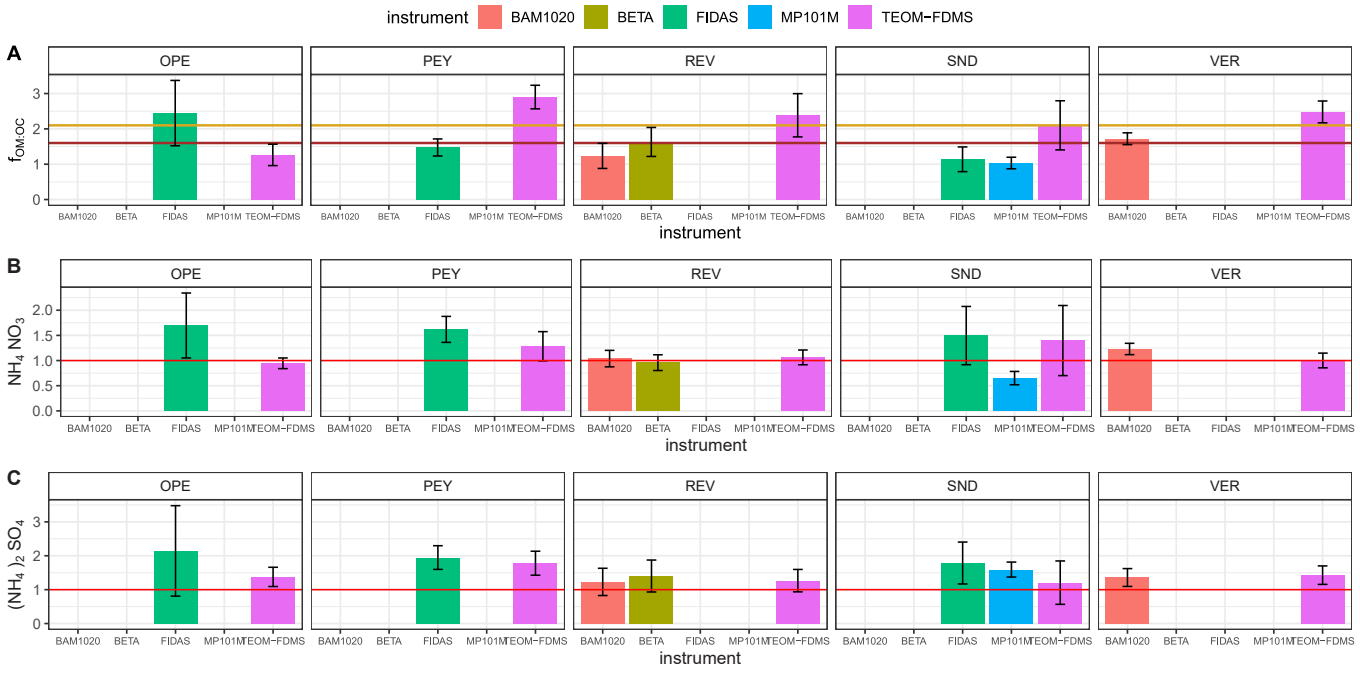

Fig. 2. Coefficients (and 95% confidence interval as error bars) resulting from the multi-linear regression #4 applied to each site and $PM_{2.5}$ instrument. The brown and yellow horizontal line in (B) corresponds to the $f_{OM:OC} = 1.6$ and $f_{OM:OC} = 2.1$ as the reference values for urban and rural sites, respectively, as per Turpin and Lim (2001). The red horizontal line in (B–C) marks the coefficient = 1.

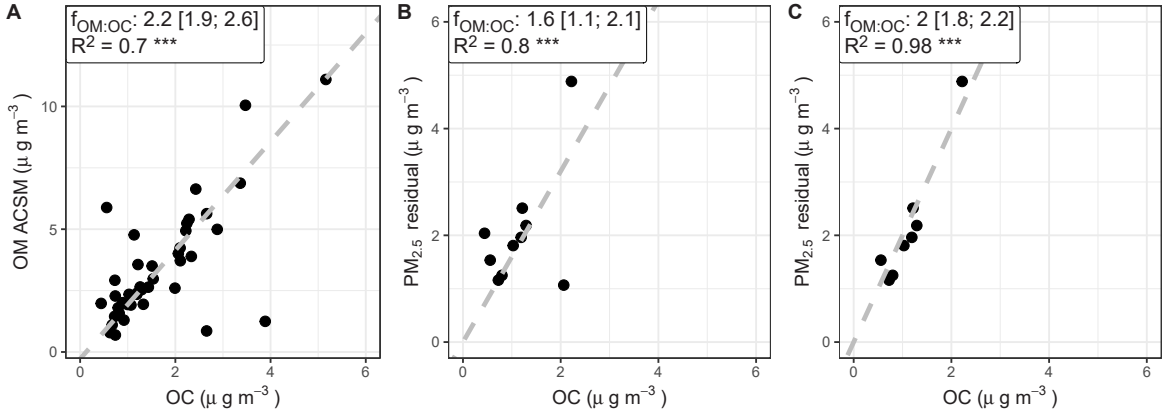

Fig. 3. Daily concentrations of OM measured by ACSM *vs* daily OC from thermo-optical determination at REV in winter 2017-18. B. $f_{OM:OC}$ calculated using the residual method from daily filters collected at REV in the same period. C. $f_{OM:OC}$ calculated using the residual method from daily filters removing those observations with $f_{OM:OC} < 0$, $f_{OM:OC} < 1$ or $f_{OM:OC} > 4$. *** statistically significant at $p < 0.001$.

residual calculation and then its subsequent exclusion as an explanatory variable in the MLR had an impact on the $f_{OM:OC}$, but not on the coefficients for AN. This may indicate that some of the artefacts associated with AS were also associated with OC. A possible explanation could be the presence of organosulphur compounds such as dimethyl sulphide (DMS) or methane sulphonic acid (MSA) which form secondary particles on filters in online instruments leading to an overestimation of $PM_{2.5}$ mass concentrations. Conversely, new particles formed from sulphuric acid and volatile organic compounds (VOCs) at these types of monitoring sites might be missed by particle counter instruments such as PALAS-FIDAS used here. Alternatively, a volatilisation of organosulphate secondary particles from the quartz filter fibres might lead to loss of $PM_{2.5}$ mass, while they would still be recovered from the chemical speciation analysis. Organosulphur compounds were estimated to account 5–10% of the organic mass at regional background sites in the US (Tolocka and Turpin, 2012); however, those are lower at European sites, of the order of 1.3% referred to total carbon (Glasius et al., 2018; Nguyen et al., 2014). However, the limited impact of AS on $f_{OM:OC}$ calculations for the BAM1020 instruments (Table 4) suggests a lower probability of the latter explanation.

The influence of AN on the determination of $f_{OM:OC}$ was estimated to be on average 4% (range: 8%–14%) as estimated from the difference in $f_{OM:OC}$ from model #5 to model #6 (Table 4).

3.4. Comparison of $f_{OM:OC}$ with aerosol mass spectra estimates

The average $f_{OM:OC}$ reported by the AMS at REV in summer 2012 was 1.8 (range: 1.7–2.0) in agreement with the summer $f_{OM:OC}$ at REV calculated from the long-term filter dataset (1.8 [1.5–2.1]; Table 3; Figure S3). In 2017-18, the $f_{OM:OC}$ ratio derived from OC from filters and

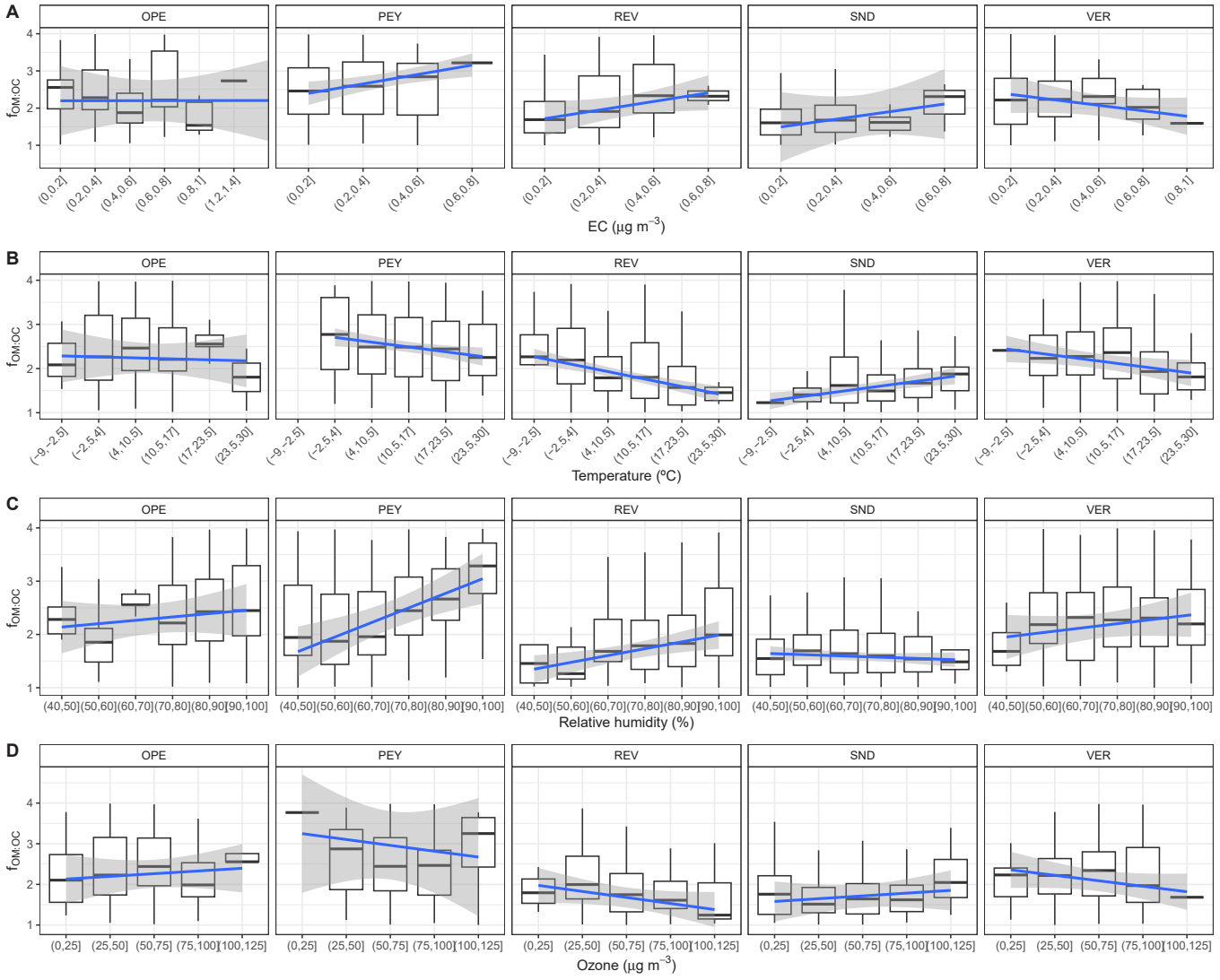

Fig. 4. Distribution of daily $f_{OM:OC}$ by bands in EC (A), temperature (B), relative humidity (C) and ozone (D) at the French rural sites. The blue line represents the OLS regression and the grey shaded area the 95% confidence interval of the linear model.

OM from Q-ACSM resulted in a slope of 2.2 (95% confidence interval: 1.9–2.6) (Table 3; Fig. 3A). This $f_{OM:OC}$ for the 2017-18 winter campaign was close to the site-specific ratio calculated from the long-term time series (2.1) (Table 3; Figure S3) but lower than the winter $f_{OM:OC}$ (2.4) for REV (Fig. S3). However, the $f_{OM:OC}$ calculated from the RM applied to filter data for the same period was 1.6 [1.1–2.1] (Fig. 3B). Removing the observations with $f_{OM:OC}$ out of the expected 1–4 range (which represented 3.2% of the data campaign), $f_{OM:OC}$ agreed with that estimated from the OM from the ACSM and was 2.0 [1.8–2.2] (Fig. 3C). $f_{OM:OC}$ was also estimated using the MLR models (models #1 to #5), and only the coefficients that where statistically significant were considered. The median value was 2.8 (range: 2.6–3.2), which was an upper limit estimate.

3.5. *Drivers of $f_{OM:OC}$ across the French rural sites*

Daily $f_{OM:OC}$ variability was related to external variables such as elemental carbon (EC), temperature (T), relative humidity (RH) and ozone (O_3). To reduce the variability of the multi-year data, this was shown in the form of boxplots (Fig. 4). Each monitoring site observed slightly different responses of $f_{OM:OC}$ against the external variables. For instance, at VER, as EC increased, $f_{OM:OC}$ decreased to values near 1.2 for EC concentrations of 0.8–1.0 μg m^{-3}, suggesting local fresh EC emissions and less oxygenated aerosols (Fig. 4A). Conversely, at PEY, REV and SND there was an increase in $f_{OM:OC}$ as EC concentrations increased suggesting the lack of local primary sources of carbonaceous aerosols and thus transported downwind to the site (Fig. 4A). The long-range transport of air masses rich in EC was then associated with aged emissions with a larger loading of oxidized aerosols. There was not a clear pattern between $f_{OM:OC}$ and EC at OPE (Fig. 4A). At PEY, REV and VER there was a reduction of $f_{OM:OC}$ from highly-oxidized values to less oxidized organic aerosols with increasing temperature (Fig. 4B). At these sites, however, there was an increase in $f_{OM:OC}$ indicating oxidized aerosols at larger RH (Fig. 4C). This might be indicative of enhance oxidation by aqueous-phase chemistry leading to the formation of SOA. Enhanced aqueous oxidation were reported previously in some single-component studies (i.e., maleic acid) (Gallimore et al., 2011). Oxalate is also formed from aqueous oxidation of several precursor compounds (see references in Ervens et al. (2011)) and it is one of the most abundant species in organic aerosol (Golly et al., 2019; Neusüss et al., 2000). However, it is important to note that the role of relative humidity is not clear in all systems (Hinks et al., 2018). The effect of the temperature on $f_{OM:OC}$ was the reverse at SND with an increase of $f_{OM:OC}$ with increasing temperature. High temperatures lead to the increase of biogenic

Table 5
Model formulation, model fit and statistical parameters (intercept and regression coefficients) of the selected linear-mixed effect model for each pollutant. Values denote the 95% confidence interval. Bold numbers indicate significance at $p < 0.05$. *** LRT test significant at $p < 0.001$.

	# 12	# 15
Formulation	$f_{OM:OC} \sim O_3 + EC + RH + (1\vert station)$	$f_{OM:OC} \sim instrument + O_3 + EC + RH + (1\vert station)$
R^2 (cAIC)^{LRT}	**0.736 (24.723)*** **	**0.676 (32.406)*** **
Intercept	**−10.1 [-17.4, -2.8]**	−5.8 [-13.8, 2.4]
O_3	**0.13 [0.07, 0.20]**	**0.10 [0.03, 0.17]**
RH	**0.07 [0.01, 0.13]**	0.04 [-0.03, 0.11]
EC	−6.0 [-19.7, 7.7]	−8.7 [-22.80, 5.40]
BETA	–	−0.02 [-1.3, 1.3]
FIDAS	–	0.61 [-0.41, 1.6]
TEOM-FDMS	–	0.11 [-1.08, 1.32]
MP101M	–	0.41 [-1.94, 1.13]

emissions of VOCs (e.g., isoprene) leading to subsequent SOA formation. The relation between $f_{OM:OC}$ and temperature was non-existent at OPE (Fig. 4B) At OPE and SND there was an increase in $f_{OM:OC}$ as O_3 concentration increased probably associated with the enhanced oxidative capacity of the atmosphere and then the oxidation of organic aerosols. The trend was reversed at PEY, REV and VER.

To understand the main drivers of $f_{OM:OC}$, linear-mixed effect models (LME) were used and related the $f_{OM:OC}$ calculated by the RM method for each instrument at each site (as shown in Fig. S5) to median EC, T, RH and O_3 for the same period. To avoid collinearity in the LME, T was excluded as explanatory variable because it showed a significant negative correlation with HR ($R = -0.87$) and a significant positive correlation with O_3 ($R = 0.75$) (Fig. S10). A total of $N = 12$ periods were considered in the LME models matching with the changes of instrumentation at each site. Different formulations were built including a null model (only with the random effect) (Table S2). The model with the best performance was model #12 with an $R^2 = 0.74$ and a cAIC value of 24.723, the latter lower to the cAIC of the null model (27.719) (Table S2). Ozone and RH were the two parameters with statistically significant impact on $f_{OM:OC}$, with an increase in $f_{OM:OC}$ of 0.13 per every μg m^{-3} of O_3; and an increase of 0.07 per every % increase in RH. Conversely, EC was associated with a decrease in $f_{OM:OC}$ but the coefficient was not statistically significant (Table 5). Therefore, both photo-oxidation and relative humidity, potentially aqueous-phase chemistry, influenced in the determination of $f_{OM:OC}$ in agreement with more oxidized OM aerosols at a larger oxidation capacity of the atmosphere.

While $f_{OM:OC}$ calculated using Eq. (9) with different type of online $PM_{2.5}$ instruments effectively resulted in different slope values (Fig. S5), the instrument was not a fixed effect on the best LME model (model #12; Table 5). Model #15 had 'instrument' as fixed effect and it was the second-best model according to the correlation coefficient ($R^2 = 0.676$) and statistically significant according to the LRT test. However, its cAIC was large (32.406) (Table S2). Any type of instrument showed statistically significant coefficients and therefore the type of instrument was not a significant factor influencing $f_{OM:OC}$ as per model #15. O_3 and RH showed similar fixed effects (0.10 per μg m^{-3}; and 0.04 per %; Table 5) compared to model #12 despite the confidence interval for RH crossed the zero value.

3.6. Mass balance calculations using tailored $f_{OM:OC}$

$PM_{2.5}$ was reconstructed using ion concentrations and using calculated $f_{OM:OC}$. An improved $PM_{2.5}$ reconstruction was achieved through site and season-specific $f_{OM:OC}$ as calculated by the RM - OLS regression forced to zero (Table 6). Reconstructed *vs* measured $PM_{2.5}$ improved at PEY from a slope of 0.68 (i.e. an underestimation of ~32%) using a fixed $f_{OM:OC}$ of 1.8 to 0.79 and to 0.88 (i.e. an underestimation of 21% and 12% of the $PM_{2.5}$ mass) using seasonal and site specific $f_{OM:OC}$, respectively. Furthermore, the mean $PM_{2.5}$ residual was 2.0 μg m^{-3} (26% error) for the fixed ratio compared to 0.69 and 0.60 μg m^{-3} (13% and 8% error) for seasonal and site-specific $f_{OM:OC}$, respectively. VER also observed an improvement of the reconstructed $PM_{2.5}$ mass, with a slope that changed from 0.84 (fixed factor) to 0.93 (both site and seasonal $f_{OM:OC}$) which represented a decrease of the unidentified mass from 13% to below 5%. The improvement for SND was notable when using a site-specific $f_{OM:OC}$, with a reduction of the residual from −11% to 0.2%. However, the use of the seasonal $f_{OM:OC}$ at SND did not show an improvement on the reconstructed $PM_{2.5}$ mass with a mean residual of 9%. REV also observed a better reconstruction of the $PM_{2.5}$ mass using the site-specific than the fixed $f_{OM:OC}$, with a mean residual representing 3% and 9% of the measured $PM_{2.5}$, respectively. Using the seasonal $f_{OM:OC}$ resulted in a better reconstruction of the $PM_{2.5}$ mass (4%) than the fixed $f_{OM:OC}$ but not compared to the site-specific one. The improvement of the $PM_{2.5}$ mass balance at OPE was less evident, with a reduction of the mean residual from 9% when using a fixed $f_{OM:OC}$; to 4% when using either site or seasonal $f_{OM:OC}$ values. For all sites, filtering the dataset and only selecting those daily samples with a $f_{OM:OC}$ in the 1–4 range as per Eq. (9), reconstructed $PM_{2.5}$ mass showed larger residuals (range from −11% to 15%) than using $f_{OM:OC}$ calculated from the full dataset (range from 0.2% to 8%) (Table 6). The use of $f_{OM:OC}$ calculated by the

Table 6
Slope of the RMA regression (±95% confidence interval) relating the reconstructed $PM_{2.5}$ mass from mass balance *vs* the measured $PM_{2.5}$ concentration. The $f_{OM:OC}$ used was a fixed value (1.8), the site-specific $f_{OM:OC}$, site-specific $f_{OM:OC}$ from selected daily observations when $f_{OM:OC}$ = 1–4; and seasonal $f_{OM:OC}$ are compared. All regressions are statistically significant at $p < 0.001$. Residual is the mean residual in μg m^{-3} and its % over total measured $PM_{2.5}$ is expressed in brackets.

		OPE	PEY	REV	SND	VER
Fixed $f_{OM:OC} = 1.8$	Slope	1.02 [0.99–1.04]	0.68 [0.66–0.70]	0.80 [0.78–0.82]	0.92 [0.90–0.94]	0.84 [0.83–0.86]
	R^2	0.78	0.71	0.78	0.71	0.88
	Residual, μg m^{-3} (%)	1.0 (9%)	2.0 (26%)	0.8 (9%)	−0.6 (−11%)	1.0 (13%)
Site specific $f_{OM:OC}$ (OLS regression)	Slope	1.02 [0.97–1.07]	0.88 [0.83–0.93]	0.86 [0.83–0.90]	0.86 [0.82–0.90]	0.93 [0.90–0.96]
	R^2	0.78	0.66	0.80	0.72	0.87
	Residual, μg m^{-3} (%)	1.0 (4%)	0.6 (8%)	0.3 (3%)	0.01 (0.2%)	0.2 (3%)
Site specific $f_{OC:OM}$ (OLS regression filtered dataset)	Slope	1.05 [1.02–1.08]	0.80 [0.78–0.83]	0.83 [0.81–0.85]	0.92 [0.90–0.95]	0.91 [0.90–0.93]
	R^2	0.78	0.68	0.77	0.71	0.87
	Residual, μg m^{-3} (%)	0.5 (5%)	1.2 (15%)	0.8 (9%)	−0.6 (−11%)	0.4 (5%)
Site specific $f_{OC:OM}$ (Multilinear regression)	Slope	1.01 [0.96; 1.06]	0.71 [0.68; 0.75]	0.81 [0.78; 0.84]	0.82 [0.78; 0.86]	0.86 [0.83; 0.89]
	R^2	0.79	0.75	0.84	0.86	0.89
	Residual, μg m^{-3} (%)	1.0 (9 %)	2.1 (27%)	1.4 (15%)	0.4 (7%)	1.0 (13%)
Seasonal $f_{OM:OC}$ (OLS regression)	Slope	1.06 [1.00–1.11]	0.79 [0.75–0.83]	0.88 [0.85–0.92]	0.92 [0.88–0.97]	0.93 [0.90–0.96]
	R^2	0.78	0.69	0.80	0.72	0.88
	Residual, μg m^{-3} (%)	0.4 (4%)	1.0 (13%)	0.4 (4%)	−0.5 (−9%)	0.4 (5%)

ensemble of the multi-linear regression as shown in Table 2 showed a general improvement of the reconstructed $PM_{2.5}$ mass compared to the fixed ratio at REV, SND and VER, with slopes ranging from 0.84 to 0.89; and mean residuals ranging from 7% to 15% (Table 6). However, the $PM_{2.5}$ mass balances using either site- or seasonal-specific ratio provided better mass closure. At OPE and PEY, the $PM_{2.5}$ reconstructed mass was similar than using a fixed ratio (Table 6).

4. Conclusions

One limitation in aerosol source apportionment studies based on the thermo-optical determination of OC is the conversion from OC to OM. Traditionally, a fixed ratio is used based on the typology of the site. However, the use of a fixed $f_{OM:OC}$ may lead to large fraction of unaccounted mass in the PM mass balance. We calculated site specific $f_{OM:OC}$, relating the residual mass with the major inorganic and OC components from daily filters, using also collocated on-line $PM_{2.5}$ measurements at one of the sites. The $PM_{2.5}$ residual was generally well-correlated to OC at all sites indicating that the unidentified chemical fraction was largely explained by OC, particularly when using the OLS regression forced to zero for this residual method (RM). Site-specific $f_{OM:OC}$ at our five French rural sites varied from 1.5 (SND) to 2.9 (PEY) over the years 2012–2021. Ratios calculated using this method on daily filter data yield comparable results to those obtained from online OM measurements at the site of REV. The use of site-specific $f_{OM:OC}$ calculated with this method for the long-term dataset resulted in better mass balance calculations, reducing the $PM_{2.5}$ unaccounted mass. When trying to define site- and season-specific $f_{OM:OC}$ and $f_{OM:OC}$ calculated removing outliers yielded larger residuals in the $PM_{2.5}$ mass balance. Further, multi-linear regression analysis was also used to derived $f_{OM:OC}$ values but the estimated values depended on the species included in the regression, and coefficients derived from these multi linear regressions were probably overestimated. Therefore, site-specific $f_{OM:OC}$ define with residual method is recommended for such exercises.

The conversion factor calculated using the RM as presented here represents, however, the upper limit of the true $f_{OM:OC}$, as the chemical speciation data used in this study does not consider metals and other minor elements. Additionally, determining $f_{OM:OC}$ using this method relies on subtracting multiple measured variables, introducing associated errors. The distribution of samples with $f_{OM:OC}$ outside the expected 1–4 range in ambient air corresponded to changes in the $PM_{2.5}$ online instrument used to monitor $PM_{2.5}$ mass concentrations. Notably, periods monitored with TEOM-FDMS yielded larger $f_{OM:OC}$ values compared to other types of instruments (e.g. BAM, FIDAS). Finally, several sampling and analytical artefacts might influence the $f_{OM:OC}$ value as assessed by the residual method. Generally, artefacts associated with ammonium sulphate were transferred to the $f_{OM:OC}$ ratio, and those represented an average increase of 16% of the $f_{OM:OC}$. Artefacts associated with ammonium sulphate were larger when particle counters are used to monitor $PM_{2.5}$ mass. Artefact associated with sulphate was also attributed to the presence of organic sulphate acids overestimating $PM_{2.5}$ mass concentrations. The literature also largely describes the artefact of volatilisation of ammonium nitrate. Here, significant artefacts associated with ammonium nitrate were only observed at one site of the five sites. Keeping the sampling system within a temperature-controlled cabin may have limited the volatilisation of ammonium nitrate at the other sites. The artefacts associated with ammonium nitrate had a minimal impact on the calculation of $f_{OM:OC}$ using the residual method, estimated at 4% on average.

The variability of $f_{OM:OC}$ at the French rural background sites underscores the lack of homogeneity across territories with apparent similar site characteristics. Both photooxidation (represented by O_3 concentrations) and aqueous-phase chemistry (represented here by the relative humidity) can influenced the value of $f_{OM:OC}$ and their influences were mathematically quantified by means of linear-mixed effect models. EC did not show a statistically significant influence on the determination of $f_{OM:OC}$. However, EC may become an important factor when considering a variety of sites including regional, rural and urban environments with distinct EC and/or fresh emission gradients. The specific type of instrument monitoring $PM_{2.5}$ mass concentrations, despite the artefacts associated with it, was not a determining factor influencing the site specific $f_{OM:OC}$ derived by the residual method.

Recently, online instruments capable of measuring the chemical composition of fine PM (mainly in PM_1 or PM with an aerodynamic diameter < 1 μm) at high time resolution (< 1 h) have become available at multiple locations across Europe (Bressi et al., 2021; Chen et al., 2022). However, historical datasets of $PM_{2.5}$ chemistry rely mainly on offline techniques. There is a critical need to ensure the consistency of the $PM_{2.5}$ chemical composition time-series and this study highlights some key elements, such as those related to OM estimates from thermo-optical OC measurements. The residual method with OLS regression forced to zero as presented here proved to be a valid method for $PM_{2.5}$ mass balance exercises. This work provides some insights in the calculation of the conversion factor, emphasizing the importance for collocated measurements of both online OM and offline filter techniques to maintain the continuity and reliability of OM estimates.

CRediT authorship contribution statement

Anna Font: Writing – original draft, Visualization, Software, Methodology, Investigation, Formal analysis, Data curation, Conceptualization. **Joel F. de Brito:** Writing – review & editing, Methodology, Investigation, Conceptualization. **Véronique Riffault:** Writing – review & editing, Validation, Resources, Methodology, Funding acquisition, Data curation, Conceptualization. **Sébastien Conil:** Writing – review & editing, Resources, Data curation. **Jean-Luc Jaffrezo:** Writing – review & editing, Validation, Resources, Methodology, Investigation, Funding acquisition, Data curation, Conceptualization. **Aude Bourin:** Writing – review & editing, Resources, Project administration, Methodology, Investigation, Funding acquisition, Data curation.

Declaration of competing interest

The authors declare that they have no known competing financial interests or personal relationships that could have appeared to influence the work reported in this paper.

Acknowledgements

This work was supported by the Ministry of Ecological Transition (MTE) and the French agency for ecological transition (ADEME); Regional Council “Hauts–de–France”. The authors would like to thank AirBreizh, Atmo Auvergne–Rhône–Alpes, Atmo Grand–Est, Atmo Occitanie and Lig’Air as well as Emmanuel Tison at IMT Nord Europe for their technical support in the field. Special thanks are given to Nicolas Bonnaire (Laboratoire des Sciences de l’Environnement et du Climat) for the laboratory analysis of ambient samples for the MERA sites; and Corentin Gouillou, Cécile Debevec and Benoît Herbin (IMT Nord Europe) for data validation of $PM_{2.5}$ mass concentration and chemical composition. The chemical analyses for the OPE data were performed at IGE on the analytical Air O Sol platform, with the work of many engineers. The 2017–2018 intensive campaign including Q-ACSM deployment at Revin was carried out as a joint effort between EMEP (https://emep.int), ACTRIS (https://www.actris.eu/) and COST COLOSSAL Action (CA16109; https://www.cost.eu/actions/CA16109/). IMT Nord Europe acknowledges financial support from the Labex CaPPA project, which is funded by the French National Research Agency (ANR) through the PIA (Programme d’Investissement d’Avenir) under contract ANR–11–LABX–0005–01, and the ECRIN project, both financed by the Regional Council “Hauts–de–France” and the European Regional Development Fund (ERDF).

Appendix A. Supplementary data

Supplementary data to this article can be found online at https://doi.org/10.1016/j.apr.2024.102301.

References

Aiken, A.C., DeCarlo, P.F., Jimenez, J.L., 2007. Elemental analysis of organic species with electron ionization high-resolution mass spectrometry. Anal. Chem. 79 (21), 8350–8358. https://doi.org/10.5194/amt-3-301-2010.

Alastuey, A., Querol, X., Aas, W., Lucarelli, F., Pérez, N., Moreno, T., Cavalli, F., Areskoug, H., Balan, V., Catrambone, M., Ceburnis, D., Cerro, J.C., Conil, S., Gevorgyan, L., Hueglin, C., Imre, K., Jaffrezo, J.L., Leeson, S.R., Mihalopoulos, N., et al., 2016. Geochemistry of PM10 over Europe during the EMEP intensive measurement periods in summer 2012 and winter 2013. Atmos. Chem. Phys. 16 (10), 6107–6129. https://doi.org/10.5194/acp-16-6107-2016.

Aslam, I., Roeffaers, M.B.J., 2022. Carbonaceous Nanoparticle air pollution: toxicity and detection in biological samples. Nanomaterials 12 (22). https://doi.org/10.3390/nano12223948.

Ayers, G.P., 2001. Comment on regression analysis of air quality data. Atmos. Environ. 35 (13), 2423–2425. https://doi.org/10.1016/S1352-2310(00)00527-6.

Bae, M.S., Demerjian, K.L., Schwab, J.J., 2006a. Seasonal estimation of organic mass to organic carbon in PM2.5 at rural and urban locations in New York state. Atmos. Environ. 40 (39), 7467–7479. https://doi.org/10.1016/j.atmosenv.2006.07.008.

Bates, D., Mächler, M., Bolker, B., Walker, S., 2015. Fitting linear mixed-effects models using lme4. J. Stat. Software 67 (1), 1–48. https://doi.org/10.18637/jss.v067.i01.

Bressi, M., Sciare, J., Ghersi, V., Bonnaire, N., Nicolas, J.B., Petit, J.-E., Moukthar, S., Rosso, A., Mihalapoulos, N., Féron, A., 2013. A one-year comprehensive chemical characterisation of fine aerosol (PM2.5) at urban, suburban and rural background sites in the region of Paris (France). Atmos. Chem. Phys. 13, 7825–7844. https://doi.org/10.5194/acp-13-7825-2013.

Bowen, H.J.M., 1979. Environmental chemistry of the elements. Academic Press.

Bressi, M., Cavalli, F., Putaud, J.P., Fröhlich, R., Petit, J.E., Aas, W., Äijälä, M., Alastuey, A., Allan, J.D., Aurela, M., Berico, M., Bougiatioti, A., Bukowiecki, N., Canonaco, F., Crenn, V., Dusanter, S., Ehn, M., Elsasser, M., Flentje, H., et al., 2021. A European aerosol phenomenology - 7: high-time resolution chemical characteristics of submicron particulate matter across Europe. Atmos. Environ. X 10 (December 2020). https://doi.org/10.1016/j.aeaoa.2021.100108.

Brown, S.G., Lee, T., Roberts, P.T., Collett, J.L., 2013. Variations in the OM/OC ratio of urban organic aerosol next to a major roadway. J. Air Waste Manag. Assoc. 63 (12), 1422–1433. https://doi.org/10.1080/10962247.2013.826602.

Carslaw, D., 2019. Package ' worldmet. https://cran.r-project.org/package=worldmet.

Cavalli, F., Viana, M., Yttri, K.E., Genberg, J., Putaud, J.-P., 2010. Toward a standardised thermal-optical protocol for measuring atmospheric organic and elemental carbon: the EUSAAR protocol. Atmos. Meas. Tech. 3, 79–89.

Cesari, D., Genga, A., Ielpo, P., Siciliano, M., Mascolo, G., Grasso, F.M., Contini, D., 2014. Source apportionment of PM2.5 in the harbour-industrial area of Brindisi (Italy): identification and estimation of the contribution of in-port ship emissions. Sci. Total Environ. 497–498, 392–400. https://doi.org/10.1016/j.scitotenv.2014.08.007.

Chebaicheb, H., Brito, J. F. De, Chen, G., Tison, E., Favez, O., Marchand, C., Pr, S.H., 2023. Investigation of four-year chemical composition and organic aerosol sources of submicron particles at the ATOLL site in northern France. Environmental Pollution 330 (May), 121805. https://doi.org/10.1016/j.envpol.2023.121805.

Chen, G., Canonaco, F., Tobler, A., Aas, W., Alastuey, A., Allan, J., Atabakhsh, S., Aurela, M., Baltensperger, U., Bougiatioti, A., De Brito, J.F., Ceburnis, D., Chazeau, B., Chebaicheb, H., Daellenbach, K.R., Ehn, M., Haddad, I. El, Eleftheriadis, K., Favez, O., Prévôt, A.S.H., 2022. European Aerosol Phenomenology – 8: Harmonised Source Apportionment of Organic Aerosol using 22 Year-long ACSM/AMS Datasets 166 (May). https://doi.org/10.1016/j.envint.2022.107325.

Chow, J.C., Lowenthal, D.H., Chen, L.W.A., Wang, X., Watson, J.G., 2015. Mass reconstruction methods for PM2.5: a review. Air Quality, Atmosphere and Health 8 (3), 243–263. https://doi.org/10.1007/s11869-015-0338-3.

Chow, J.C., Riggio, G.M., Wang, X., Chen, L.W.A., Watson, J.G., 2018. Measuring the organic carbon to organic matter multiplier with thermal/optical carbon-quadrupole mass spectrometer analyses. Aerosol Science and Engineering 2 (4), 165–172. https://doi.org/10.1007/s41810-018-0033-5.

Christiansen, A.E., Carlton, A.G., Porter, W.C., 2020. Changing nature of organic carbon over the United States. Environ. Sci. Technol. 54 (17), 10524–10532. https://doi.org/10.1021/acs.est.0c02225.

Cozic, J., Verheggen, B., Weingartner, E., Crosier, J., Bower, K.N., Flynn, M., Coe, H., Henning, S., Steinbacher, M., Henne, S., Coen, M.C., Petzold, A., Baltensperger, U., 2008. Atmospheric Chemistry and Physics Chemical composition of free tropospheric aerosol for PM1 and coarse mode at the high alpine site Jungfraujoch. Atmos. Chem. Phys. 8. www.atmos-chem-phys.net/8/407/2008/.

Crippa, M., El Haddad, I., Slowik, J.G., Decarlo, P.F., Mohr, C., Heringa, M.F., Chirico, R., Marchand, N., Sciare, J., Baltensperger, U., Prévôt, A.S.H., 2013. Identification of marine and continental aerosol sources in Paris using high resolution aerosol mass spectrometry. J. Geophys. Res. Atmos. 118 (4), 1950–1963. https://doi.org/10.1002/jgrd.50151.

Daellenbach, K.R., Stefenelli, G., Bozzetti, C., Vlachou, A., Fermo, P., Gonzalez, R., Piazzalunga, A., Colombi, C., Canonaco, F., Hueglin, C., Kasper-Giebl, A., Jaffrezo, J. L., Bianchi, F., Slowik, J.G., Baltensperger, U., El-Haddad, I., Prévôt, A.S.H., 2017. Long-term chemical analysis and organic aerosol source apportionment at nine sites in central Europe: source identification and uncertainty assessment. Atmos. Chem. Phys. 17 (21), 13265–13282. https://doi.org/10.5194/acp-17-13265-2017.

Dormann, C.F., Elith, J., Bacher, S., Buchmann, C., Carl, G., Carré, G., Marquéz, J.R.G., Gruber, B., Lafourcade, B., Leitão, P.J., Münkemüller, T., Mcclean, C., Osborne, P.E., Reineking, B., Schröder, B., Skidmore, A.K., Zurell, D., Lautenbach, S., 2013. Collinearity: a review of methods to deal with it and a simulation study evaluating their performance. Ecography 36 (1), 27–46. https://doi.org/10.1111/j.1600-0587.2012.07348.x.

El-Zanan, H.S., Lowenthal, D.H., Zielinska, B., Chow, J.C., Kumar, N., 2005. Determination of the organic aerosol mass to organic carbon ratio in IMPROVE samples. Chemosphere 60 (4), 485–496. https://doi.org/10.1016/j.chemosphere.2005.01.005.

Ervens, B., Turpin, B.J., Weber, R.J., 2011. Secondary organic aerosol formation in cloud droplets and aqueous particles (aqSOA): a review of laboratory, field and model studies. Atmos. Chem. Phys. 11 (21), 11069–11102. https://doi.org/10.5194/acp-11-11069-2011.

European Parliament, & Council of the European Union, 2008. Directive 2008/50/EC of the European Parliament and of the Council of 21 May 2008 on ambient air quality and cleaner air for Europe. Official Journal of the European Communities 1–43. http://eur-lex.europa.eu/LexUriServ/LexUriServ.do?uri=OJ:L:2008:152:0001:0044:EN:PDF.

Favez, O., Weber, S., Petit, J.E., Alleman, L.Y., Albinet, A., Riffault, V., Chazeau, B., Amodeo, T., Salameh, D., Zhang, Y., Srivastava, D., Samaké, A., Aujay-Plouzeau, R., Papin, A., Bonnaire, N., Boullanger, C., Chatain, M., Chevrier, F., Detournay, A., et al., 2021. Overview of the French operational network for in situ observation of PM chemical composition and sources in urban environments (CARA program). Atmosphere 12 (2). https://doi.org/10.3390/atmos12020207.

Font, A., de Brito, J.F., Riffault, V., Conil, S., Jaffrezo, J.L., Bourin, A., 2024. Long-term measurements of aerosol composition at rural background sites in France: Sources, seasonality and mass closure of PM2.5. Atmos. Environ. 334. https://doi.org/10.1016/j.atmosenv.2024.120724.

Galindo, N., Yubero, E., Clemente, Á., Nicolás, J.F., Varea, M., Crespo, J., 2020. PM events and changes in the chemical composition of urban aerosols: a case study in the western Mediterranean. Chemosphere 244. https://doi.org/10.1016/j.chemosphere.2019.125520.

Gallimore, P.J., Achakulwisut, P., Pope, F.D., Davies, J.F., Spring, D.R., Kalberer, M., 2011. Importance of relative humidity in the oxidative ageing of organic aerosols: case study of the ozonolysis of maleic acid aerosol. Atmos. Chem. Phys. 11 (23), 12181–12195. https://doi.org/10.5194/acp-11-12181-2011.

Glasius, M., Hansen, A.M.K., Claeys, M., Henzing, J.S., Jedynska, A.D., Kasper-Giebl, A., Kistler, M., Kristensen, K., Martinsson, J., Maenhaut, W., Nøjgaard, J.K., Spindler, G., Stenström, K.E., Swietlicki, E., Szidat, S., Simpson, D., Yttri, K.E., 2018. Composition and sources of carbonaceous aerosols in Northern Europe during winter. Atmos. Environ. 173, 127–141 j.atmosenv.

Golly, B., Waked, A., Weber, S., Samake, A., Jacob, V., Conil, S., Rangognio, J., Chrétien, E., Vagnot, M.P., Robic, P.Y., Besombes, J.L., Jaffrezo, J.L., 2019. Organic markers and OC source apportionment for seasonal variations of PM2.5 at 5 rural sites in France. Atmos. Environ. 198, 142–157. https://doi.org/10.1016/j.atmosenv.2018.10.027.

Guinot, B., Cachier, H., Oikonomou, K., 2007. Geochemical perspectives from a new aerosol chemical mass closure. Atmos. Chem. Phys. 7 (6), 1657–1670. https://doi.org/10.5194/acp-7-1657-2007.

Hand, J.L., Prenni, A.J., Schichtel, B.A., Malm, W.C., Chow, J.C., 2019. Trends in remote PM2.5 residual mass across the United States: implications for aerosol mass reconstruction in the IMPROVE network. Atmos. Environ. 203 (November 2018), 141–152. https://doi.org/10.1016/j.atmosenv.2019.01.049.

He, L., Chen, H., Rangognio, J., Yahyaoui, A., Colin, P., Wang, J., Daële, V., Mellouki, A., 2018. Fine particles at a background site in Central France: chemical compositions, seasonal variations and pollution events. Sci. Total Environ. 612, 1159–1170. https://doi.org/10.1016/j.scitotenv.2017.08.273.

Hennigan, C.J., Bergin, M.H., Russell, A.G., Nenes, A., Weber, R.J., 2009. Atmospheric Chemistry and Physics Gas/particle partitioning of water-soluble organic aerosol in Atlanta. Atmos. Chem. Phys. 9. www.atmos-chem-phys.net/9/3613/2009/.

Hinks, M.L., Montoya-Aguilera, J., Ellison, L., Lin, P., Laskin, A., Laskin, J., Shiraiwa, M., Dabdub, D., Nizkorodov, S.A., 2018. Effect of relative humidity on the composition of secondary organic aerosol from the oxidation of toluene. Atmos. Chem. Phys. 18 (3), 1643–1652. https://doi.org/10.5194/acp-18-1643-2018.

IPCC, 2021. Climate Change 2021: The Physical Science Basis. Contribution of Working Group I to the Sixth Assessment Report of the Intergovernmental Panel on Climate Change. Cambridge University Press. In Press, 3949. https://www.ipcc.ch/report/ar6/wg1/downloads/report/IPCC_AR6_WGI_Full_Report.pdf.

Janssen, N.A., Gerlofs-Nijland, M.E., Lanki, T., Salonen, R.O., Cassee, F., Hoek, G., Fischer, P., Brunekreef, B., Krzyzanowski, M., 2012. Health Effects of Black Carbon. *World Health*.

Keck, L., Wittmaack, K., 2005. Effect of filter type and temperature on volatilisation losses from ammonium salts in aerosol matter. Atmos. Environ. 39 (22), 4093–4100. https://doi.org/10.1016/j.atmosenv.2005.03.029.

Kiss, G., Varga, B., Galambos, I., Ganszky, I., 2002. Characterization of water-soluble organic matter isolated from atmospheric fine aerosol. J. Geophys. Res. Atmos. 107 (21) https://doi.org/10.1029/2001JD000603.

LCSQA, 2013. LCSQA, Métrologie des particules. http://www.lcsqa.org/rapport/2012/ineris/suivi-optimisation-utilisation-teom-fdms-bilan.

LCSQA, 2017. Vérification de la conformité technique des appareils de mesure pour la surveillance réglementaire de la qualité de l'air. https://imt-nord-europe.hal.science/hal-04250464.

Le, T.C., Shukla, K.K., Chen, Y.T., Chang, S.C., Lin, T.Y., Li, Z., Pui, D.Y.H., Tsai, C.J., 2020. On the concentration differences between PM2.5 FEM monitors and FRM samplers. Atmos. Environ. 222 https://doi.org/10.1016/j.atmosenv.2019.117138.

Lim, H.-J., Turpin, B.J., 2002. Origins of primary and secondary organic aerosol in Atlanta: results of time-resolved measurements during the Atlanta Supersite Experiment. Environ. Sci. Technol. 36 (21), 4489–4496. https://doi.org/10.1021/es0206487.

Liu, C.N., Awasthi, A., Hung, Y.H., Gugamsetty, B., Tsai, C.J., Wu, Y.C., Chen, C.F., 2013. Differences in 24-h average PM2.5 concentrations between the beta attenuation monitor (BAM) and the dichotomous sampler (Dichot). Atmos. Environ. 75, 341–347. https://doi.org/10.1016/j.atmosenv.2013.04.062.

Liu, X., Henzing, B., Hensen, A., Mulder, J., Yao, P., Van Dinther, D., Van Bronckhorst, J., Huang, R., Dusek, U., 2024. Measurement report: Evaluation of the TOF-ACSM-CV for PM1.0 and PM2.5 measurements during the RITA-2021 field campaign. Atmos. Chem. Phys. 24 (6), 3405–3420. https://doi.org/10.5194/acp-24-3405-2024.

Lowenthal, D., Zielinska, B., Mason, B., Samy, S., Samburova, V., Collins, D., Spencer, C., Taylor, N., Allen, J., Kumar, N., 2009. Aerosol characterization studies at great smoky mountains national park, summer 2006. J. Geophys. Res. Atmos. 114 (8) https://doi.org/10.1029/2008JD011274.

Malm, W.C., Hand, J.L., 2007. An examination of the physical and optical properties of aerosols collected in the IMPROVE program. Atmos. Environ. 41 (16), 3407–3427. https://doi.org/10.1016/j.atmosenv.2006.12.012.

Malm, W.C., Schichtel, B.A., Pitchford, M.L., 2011. Uncertainties in PM2.5 gravimetric and speciation measurements and what we can learn from them. J. Air Waste Manag. Assoc. 61 (11), 1131–1149. https://doi.org/10.1080/10473289.2011.603998.

Marconi, M., Sferlazzo, D.M., Becagli, S., Bommarito, C., Calzolai, G., Chiari, M., di Sarra, A., Ghedini, C., Gómez-Amo, J.L., Lucarelli, F., Meloni, D., Monteleone, F., Nava, S., Pace, G., Piacentino, S., Rugi, F., Severi, M., Traversi, R., Udisti, R., 2014. Saharan dust aerosol over the central Mediterranean Sea: PM10 chemical composition and concentration versus optical columnar measurements. Atmos. Chem. Phys. 14, 2039–2054. https://doi.org/10.5194/acp-14-2039-2014.

Mauderly, J.L., Chow, J.C., 2008. Health effects of organic aerosols. Inhal. Toxicol. 20 (Issue 3) https://doi.org/10.1080/08958370701866008.

Mohr, C., DeCarlo, P.F., Heringa, M.F., Chirico, R., Slowik, J.G., Richter, R., Reche, C., Alastuey, A., Querol, X., Seco, R., Peñuelas, J., Jiḿenez, J.L., Crippa, M., Zimmermann, R., Baltensperger, U., 2012. Identification and quantification of organic aerosol from cooking and other sources in Barcelona using aerosol mass spectrometer data. Atmos. Chem. Phys. 12 (4), 1649–1665. https://doi.org/10.5194/acp-12-1649-2012.

Neusüss, C., Pelzing, M., Plewka, A., Herrmann, H., 2000. A new analytical approach for size-resolved speciation of organic compounds in atmospheric aerosol particles: methods and first results. J. Geophys. Res. Atmos. 105 (D4), 4513–4527. https://doi.org/10.1029/1999JD901038.

Ng, N.L., Herndon, S.C., Trimborn, A., Canagaratna, M.R., Croteau, P.L., Onasch, T.B., Sueper, D., Worsnop, D.R., Zhang, Q., Sun, Y.L., Jayne, J.T., 2011. An Aerosol Chemical Speciation Monitor (ACSM) for routine monitoring of the composition and mass concentrations of ambient aerosol. Aerosol. Sci. Technol. 45 (7), 780–794. https://doi.org/10.1080/02786826.2011.560211.

Nguyen, Q.T., Christensen, M.K., Cozzi, F., Zare, A., Hansen, A.M.K., Kristensen, K., Tulinius, T.E., Madsen, H.H., Christensen, J.H., Brandt, J., Massling, A., Nøjgaard, J. K., Glasius, M., 2014. Understanding the anthropogenic influence on formation of biogenic secondary organic aerosols in Denmark via analysis of organosulfates and related oxidation products. Atmos. Chem. Phys. 14 (17), 8961–8981. https://doi.org/10.5194/acp-14-8961-2014.

Park, R.J., Jacob, D.J., Chin, M., Martin, R.V., 2003. Sources of carbonaceous aerosols over the United States and implications for natural visibility. J. Geophys. Res. Atmos. 108 (12) https://doi.org/10.1029/2002jd003190.

Petit, J.E., Favez, O., Sciare, J., Crenn, V., Sarda-Estève, R., Bonnaire, N., Močnik, G., Dupont, J.C., Haeffelin, M., Leoz-Garziandia, E., 2015. Two years of near real-time chemical composition of submicron aerosols in the region of Paris using an Aerosol Chemical Speciation Monitor (ACSM) and a multi-wavelength Aethalometer. Atmos. Chem. Phys. 15 (6), 2985–3005. https://doi.org/10.5194/acp-15-2985-2015.

Pio, C., Alves, C., Nunes, T., Cerqueira, M., Lucarelli, F., Nava, S., Calzolai, G., Gianelle, V., Colombi, C., Amato, F., Karanasiou, A., Querol, X., 2020. Source apportionment of PM2.5 and PM10 by Ionic and Mass Balance (IMB) in a traffic-influenced urban atmosphere, in Portugal. Atmos. Environ. 223, 117217. https://doi.org/10.1016/j.atmosenv.2019.117217.

Polidori, A., Turpin, B.J., Rodenburg, L.A., Maimone, F., Davidson, C.I., 2008. Organic pm2.5: fractionation by polarity, ftir spectroscopy, and om/oc ratio for the pittsburgh aerosol. Aerosol. Sci. Technol. 42 (3), 233–246. https://doi.org/10.1080/02786820801958767.

Poulain, L., Spindler, G., Grüner, A., Tuch, T., Stieger, B., Pinxteren, D. Van, Petit, J.E., Favez, O., Herrmann, H., Wiedensohler, A., 2020. Multi-year ACSM measurements at the central European research station Melpitz (Germany) - Part 1: instrument robustness, quality assurance, and impact of upper size cutoff diameter. Atmos. Meas. Tech. 13 (9), 4973–4994. https://doi.org/10.5194/amt-13-4973-2020.

Querol, X., Alastuey, A., Viana, M., Moreno, T., Reche, C., Minguillón, M.C., Ripoll, A., Pandolfi, M., Amato, F., Karanasiou, A., Pérez, N., Pey, J., Cusack, M., Vázquez, R., Plana, F., Dall'Osto, M., De La Rosa, J., Sánchez De La Campa, A., Fernández-Camacho, R., et al., 2013. Variability of carbonaceous aerosols in remote, rural, urban and industrial environments in Spain: implications for air quality policy. Atmos. Chem. Phys. 13 (13), 6185–6206. https://doi.org/10.5194/acp-13-6185-2013.

Roig Rodelas, R., Chakraborty, A., Perdrix, E., Tison, E., Riffault, V., 2019. Real-time assessment of wintertime organic aerosol characteristics and sources at a suburban site in northern France. Atmos. Environ. 203, 48–61. https://doi.org/10.1016/j.atmosenv.2019.01.035.

Ruthenburg, T.C., Perlin, P.C., Liu, V., McDade, C.E., Dillner, A.M., 2014. Determination of organic matter and organic matter to organic carbon ratios by infrared spectroscopy with application to selected sites in the IMPROVE network. Atmos. Environ. 86, 47–57. https://doi.org/10.1016/j.atmosenv.2013.12.034.

Salvador, C.M., Chou, C.C.K., 2014. Analysis of semi-volatile materials (SVM) in fine particulate matter. Atmos. Environ. 95, 288–295. https://doi.org/10.1016/j.atmosenv.2014.06.046.

Schwab, J.J., Felton, H.D., Rattigan, O.V., Demerjian, K.L., 2006. New York state urban and rural measurements of continuous PM2.5Mass by FDMS, TEOM, and BAM. J. Air Waste Manag. Assoc. 56 (4), 372–383. https://doi.org/10.1080/10473289.2006.10464523.

Sciare, J., Cachier, H., Oikonomou, K., Ausset, P., Sarda-Esteve, R., Mihalopoulos, N., 2003. Characterization of carbonaceous aerosols during the MINOS campaign in Crete, July-August 2001: a multi-analytical approach. Atmos. Chem. Phys. 3, 1743–1757. https://doi.org/10.5194/acpd-3-3373-2003.

Seinfeld, J.H., Pandis, S.N., 2006. ATMOSPHERIC from air pollution to climate change SECOND EDITION. Atmos. Chem. Phys.

Seinfeld, J.H., Pankow, J.F., 2003. Organic atmospheric particulate material. Annu. Rev. Phys. Chem. 54, 121–140. https://doi.org/10.1146/annurev.physchem.54.011002.103756.

Simon, H., Bhave, P.V., Swall, J.L., Frank, N.H., Malm, W.C., 2011. Determining the spatial and seasonal variability in OM/OC ratios across the US using multiple regression. Atmos. Chem. Phys. 11 (6), 2933–2949. https://doi.org/10.5194/acp-11-2933-2011.

Smith, A., Lott, N., Vose, R., 2011. The integrated surface database: recent developments and partnerships. Bull. Am. Meteorol. Soc. 92 (6), 704–708. https://doi.org/10.1175/2011BAMS3015.1.

Srivastava, D., Vu, T.V., Tong, S., Shi, Z., Harrison, R.M., 2022. Formation of secondary organic aerosols from anthropogenic precursors in laboratory studies. Npj Climate and Atmospheric Science 5 (1). https://doi.org/10.1038/s41612-022-00238-6.

Takahama, S., Schwartz, R.E., Russell, L.M., MacDonald, A.M., Sharma, S., Leaitch, W.R., 2011. Organic functional groups in aerosol particles from burning and non-burning forest emissions at a high-elevation mountain site. Atmos. Chem. Phys. 11 (13), 6367–6386. https://doi.org/10.5194/acp-11-6367-2011.

Timonen, H., Carbone, S., Aurela, M., Saarnio, K., Saarikoski, S., Ng, N.L., Canagaratna, M.R., Kulmala, M., Kerminen, V., Worsnop, D.R., Hillamo, R., 2013. Characteristics , sources and water-solubility of ambient submicron organic aerosol in springtime in Helsinki , Finland. J. Aerosol Sci. 56, 61–77. https://doi.org/10.1016/j.jaerosci.2012.06.005.

Tolocka, M.P., Turpin, B., 2012. Contribution of organosulfur compounds to organic aerosol mass. Environ. Sci. Technol. 46 (15), 7978–7983. https://doi.org/10.1021/es300651v.

Turpin, B.J., Lim, H.-J., 2001. Species contributions to PM2.5 mass concentrations: revisiting common assumptions for estimating organic mass. Aerosol. Sci. Technol. 35 (1), 602–610. https://doi.org/10.1080/02786820119445.

Viana, M., Chi, X., Maenhaut, W., Cafmeyer, J., Querol, X., Alastuey, a., Mikuška, P., Večeřa, Z., 2006. Influence of sampling artefacts on measured PM, OC, and EC levels in carbonaceous aerosols in an urban area. Aerosol Sci. Technol. 40 (2), 107–117. https://doi.org/10.1080/02786820500484388.

Wallace, H.W., Sanchez, N.P., Flynn, J.H., Erickson, M.H., Lefer, B.L., Griffin, R.J., 2018. Source apportionment of particulate matter and trace gases near a major refinery near the Houston Ship Channel. Atmos. Environ. 173, 16–29. https://doi.org/10.1016/j.atmosenv.2017.10.049.

Weber, S., Salameh, D., Albinet, A., Alleman, L.Y., Waked, A., Besombes, J.L., Jacob, V., Guillaud, G., Meshbah, B., Rocq, B., Hulin, A., Dominik-Sègue, M., Chrétien, E., Jaffrezo, J.L., Favez, O., 2019. Comparison of PM10 sources profiles at 15 French sites using a harmonized constrained positive matrix factorization approach. Atmosphere 10 (6), 1–22. https://doi.org/10.3390/atmos10060310.

Yttri, K.E., Dye, C., Braathen, O. -a., Simpson, D., Steinnes, E., 2009. Carbonaceous aerosols in Norwegian urban areas. Atmos. Chem. Phys. 9 (6), 2007–2020. https://doi.org/10.5194/acp-9-2007-2009.

Yttri, K.E., Canonaco, F., Eckhardt, S., Evangeliou, N., Fiebig, M., Gundersen, H., Hjellbrekke, A.G., Lund Myhre, C., Matthew Platt, S., Prevot, A.S.H., Simpson, D., Solberg, S., Surratt, J., Tørseth, K., Uggerud, H., Vadset, M., Wan, X., Aas, W., 2021. Trends, composition, and sources of carbonaceous aerosol at the Birkenes Observatory, northern Europe, 2001-2018. Atmos. Chem. Phys. 21 (9), 7149–7170. https://doi.org/10.5194/acp-21-7149-2021.